

1    **Functional analysis of the fatty acid and alcohol metabolism of *Pseudomonas putida* using**  
2    **RB-TnSeq**

3    Mitchell G. Thompson<sup>1,2,3\*</sup>, Matthew R. Incha<sup>1,2,4\*</sup>, Allison N. Pearson<sup>1,2,4\*</sup>, Matthias  
4    Schmidt<sup>1,2,5</sup>, William A. Sharpless<sup>1,2</sup>, Christopher B. Eiben<sup>1,2,6</sup>, Pablo Cruz-Morales<sup>1,2,7</sup>,  
5    Jacquelyn M. Blake-Hedges<sup>1,2,8</sup>, Yuzhong Liu<sup>1,2</sup>, Catharine A. Adams<sup>2</sup>, Robert W. Haushalter<sup>1,2</sup>,  
6    Rohith N. Krishna<sup>1,2</sup>, Patrick Lichtner<sup>1,2</sup>, Lars M. Blank<sup>5</sup>, Aindrla Mukhopadhyay<sup>1,2</sup>, Adam M.  
7    Deutschbauer<sup>4,9</sup>, Patrick M. Shih<sup>1,2,3,10#</sup>, Jay D. Keasling<sup>1,2,6,11,12,13,14#</sup>

8  
9   <sup>1</sup>Joint BioEnergy Institute, 5885 Hollis Street, Emeryville, CA 94608, USA.

10   <sup>2</sup>Biological Systems & Engineering Division, Lawrence Berkeley National Laboratory, Berkeley,  
11   CA 94720, USA.

12   <sup>3</sup>Department of Plant Biology, University of California, Davis, CA 95616, USA

13   <sup>4</sup>Department of Plant and Microbial Biology, University of California, Berkeley, CA 94720,  
14   USA

15   <sup>5</sup>Institute of Applied Microbiology-iAMB, Aachen Biology and Biotechnology-ABBt, RWTH  
16   Aachen University, Aachen, Germany

17   <sup>6</sup>Joint Program in Bioengineering, University of California, Berkeley/San Francisco, CA 94720,  
18   USA

19   <sup>7</sup>Centro de Biotecnología FEMSA, Instituto Tecnológico y de Estudios superiores de Monterrey,  
20   México

21   <sup>8</sup>Department of Chemistry, University of California, Berkeley, CA 94720, USA

22   <sup>9</sup>Environmental Genomics and Systems Biology Division, Lawrence Berkeley National  
23   Laboratory, Berkeley, California, USA

24   <sup>10</sup>Environmental and Genomics and Systems Biology Division, Lawrence Berkeley National  
25   Laboratory, Berkeley, CA 94720, USA.

26   <sup>11</sup>Department of Chemical and Biomolecular Engineering, University of California, Berkeley,  
27   CA 94720, USA

28   <sup>12</sup>Institute for Quantitative Biosciences, University of California, Berkeley, CA 94720, USA

29   <sup>13</sup>The Novo Nordisk Foundation Center for Biosustainability, Technical University of Denmark,  
30   Denmark

31   <sup>14</sup>Center for Synthetic Biochemistry, Institute for Synthetic Biology, Shenzhen Institutes for  
32   Advanced Technologies, Shenzhen, China

33  
34   \*Authors contributed equally

35

36   #Co-corresponding authors

37   Jay D. Keasling, jdkeasling@lbl.gov

38   Patrick M. Shih, pmshih@lbl.gov

39

40

41

42 **ABSTRACT**

43 With its ability to catabolize a wide variety of carbon sources and a growing engineering  
44 toolkit, *Pseudomonas putida* KT2440 is emerging as an important chassis organism for  
45 metabolic engineering. Despite advances in our understanding of this organism, many gaps  
46 remain in our knowledge of the genetic basis of its metabolic capabilities. These gaps are  
47 particularly noticeable in our understanding of both fatty acid and alcohol catabolism, where  
48 many paralogs putatively coding for similar enzymes co-exist making biochemical assignment  
49 via sequence homology difficult. To rapidly assign function to the enzymes responsible for these  
50 metabolisms, we leveraged Random Barcode Transposon Sequencing (RB-TnSeq). Global  
51 fitness analyses of transposon libraries grown on 13 fatty acids and 10 alcohols produced strong  
52 phenotypes for hundreds of genes. Fitness data from mutant pools grown on varying chain length  
53 fatty acids indicated specific enzyme substrate preferences, and enabled us to hypothesize that  
54 DUF1302/DUF1329 family proteins potentially function as esterases. From the data we also  
55 postulate catabolic routes for the two biogasoline molecules isoprenol and isopentanol, which are  
56 catabolized via leucine metabolism after initial oxidation and activation with CoA. Because fatty  
57 acids and alcohols may serve as both feedstocks or final products of metabolic engineering  
58 efforts, the fitness data presented here will help guide future genomic modifications towards  
59 higher titers, rates, and yields.

60

61

62

63

64 **IMPORTANCE**

65 To engineer novel metabolic pathways into *P. putida*, a comprehensive understanding of  
66 the genetic basis of its versatile metabolism is essential. Here we provide functional evidence for  
67 the putative roles of hundreds of genes involved in the fatty acid and alcohol metabolism of this  
68 bacterium. These data provide a framework facilitating precise genetic changes to prevent  
69 product degradation and channel the flux of specific pathway intermediates as desired.

70

## 71 INTRODUCTION

72 *Pseudomonas putida* KT2440 is an important metabolic engineering chassis, which can  
73 readily metabolize compounds derived from lignocellulosic and plastic derived feedstocks (1–3),  
74 and has an ever-growing repertoire of advanced tools for genome modification (4–7). Its upper  
75 glycolytic pathway architecture enables *P. putida* to natively generate large amounts of reducing  
76 equivalent (8), and it more robustly withstands metabolic burdens than many other frequently  
77 used host organisms (9). To date, a wide variety of products have been produced through  
78 metabolic engineering of *P. putida*, including valerolactam (10), curcuminoids (11), diacids (12),  
79 methyl-ketones (13), rhamnolipids (14), cis,cis-muconic acid (15), and many others (16). Recent  
80 advances in genome-scale metabolic modeling of *P. putida* make engineering efforts more  
81 efficient (7, 17). However, a large gap still exists between genes predicted to encode enzymatic  
82 activity and functional data to support these assumptions. Recent characterizations of enzymes  
83 and transporters involved in the catabolism of lysine (12, 18), levulinic acid (19), and aromatic  
84 compounds (20) highlight the need to continue functionally probing the metabolic capabilities of  
85 *P. putida*, because its native catabolism can consume many target molecules and dramatically  
86 impact titers.

87 Amongst the most important metabolisms not yet rigorously interrogated via omics-level  
88 analyses are fatty acid and alcohol degradation. Recently, fatty acids have been shown to be a  
89 non-trivial component of some feedstock streams (1) and, depending on their chain length, serve  
90 as high-value target molecules (21). Furthermore, intermediates in beta-oxidation can be  
91 channeled towards mega-synthases to produce more complex molecules (22), or used in reverse  
92 beta-oxidation to produce compounds such as medium chain n-alcohols (23). However,  
93 assigning the genetic basis of fatty acid degradation is complicated by the presence of multiple  
94 homologs of the individual *fad* genes encoded in the genome of *P. putida* KT2440 (17, 24).  
95 Although work has been done to either biochemically or genetically demonstrate the substrate  
96 specificity of some individual *fad* genes, the majority of these homologs still have no functional  
97 data associated with them.

98 *P. putida* is also able to oxidize and catabolize a wide variety of alcohols. Much work has  
99 focused on the unique biochemistry and regulation of two pyrroloquinoline quinone (PQQ)-  
100 dependent alcohol dehydrogenases (ADH), *pedE* and *pedH*, which exhibit broad substrate  
101 specificity for both alcohols and aldehydes (25, 26). Specific work has also investigated the  
102 suitability of *P. putida* for the production of ethanol (27) and the genetic basis for its ability to  
103 catabolize butanol and 1,4-butanediol (28–30). *P. putida* is also known for its ability to tolerate  
104 solvents and alcohols, making it an attractive host for their industrial production (31, 32).  
105 Tolerance to these compounds is a product of both robust efflux pumps (31) and the ability of  
106 some strains, such as *P. putida* mt-2, to catabolize a range of organic compounds (33). Metabolic  
107 engineering has biologically produced a diverse range of alcohols with a wide array of industrial  
108 and commercial uses (34–36). As more alcohol synthesis pathways are engineered into *P. putida*,

109 a more complete understanding of the molecular basis of its catabolic capacities will be required  
110 to achieve high-titers.

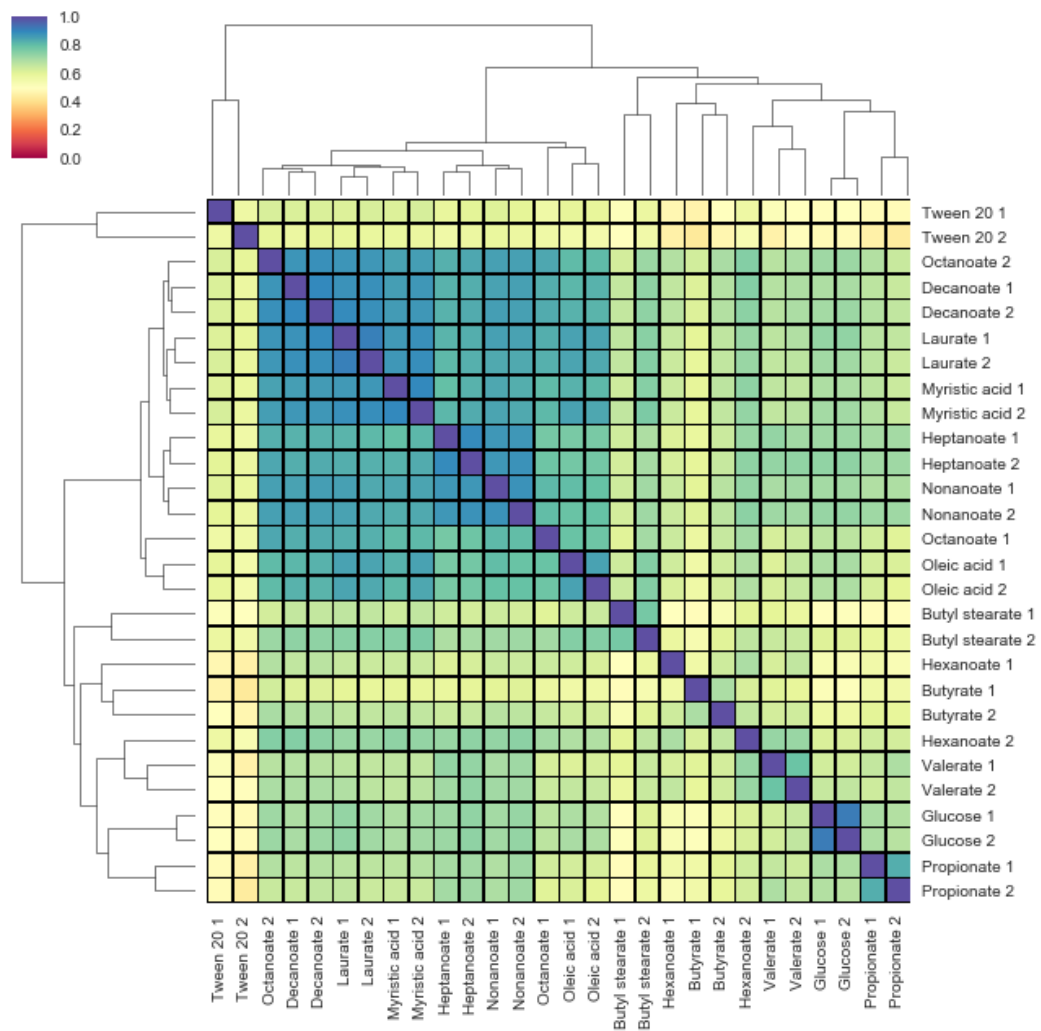
111 A recent surge in omics-level data has revealed much about the metabolism of *P. putida*,  
112 with adaptive evolution (30), proteomics (10, 28, 29), and  $^{13}\text{C}$  flux analysis (37–39) yielding  
113 valuable insights. An approach that has proven to be particularly powerful is Random Barcode  
114 Transposon Sequencing (RB-TnSeq) (40, 41). RB-TnSeq allows rapid and inexpensive genome-  
115 wide profiling of individual gene fitness in various conditions, and has been used in *P. putida* to  
116 identify numerous novel metabolic pathways and aid in increasing titers of the polymer precursor  
117 valerolactam (10, 11, 18–20). Here, we leverage RB-TnSeq to interrogate the genetic basis for  
118 the catabolism of multiple fatty acids and alcohols to develop an evidence-based understanding  
119 of the enzymes and pathways utilized in these metabolisms.

120

## 121 RESULTS AND DISCUSSION

122 **Global Analysis of Fatty Acid Metabolism.** To characterize the genetic basis of fatty acid  
123 metabolism in *P. putida*, barcoded transposon mutant libraries were grown in minimal media  
124 with straight chain fatty acids (C3-C10, C12, and C14), fatty esters (Tween20 and butyl stearate),  
125 and an unsaturated fatty acid (oleic acid) as sole carbon sources. Pearson correlation analyses of  
126 global fitness patterns revealed that the metabolisms of straight chain fatty acids between C7 and  
127 C14 clade together, suggesting similar overall catabolic routes (**Figure 1**). Oleic acid, an 18-  
128 carbon monounsaturated fatty acid, also grouped within this clade. Shorter chain fatty acids  
129 (<C7) did not show high correlation to one another based on global fitness analyses, suggesting  
130 more independent routes of catabolism (**Figure 1**). Annotations in the BioCyc database,  
131 functional assignment from a recent metabolic model of *P. putida* KT440 (*iJN1462*), and

132 previous *in vitro* biochemical work predict the existence of several enzymes in the genome of the  
133 bacterium that may be putatively involved in fatty acid catabolism: six acyl-CoA ligases, seven  
134 acyl-CoA dehydrogenases, seven enoyl-CoA hydratases, four hydroxyacyl-CoA dehydrogenases,  
135 and five thiolases (**Figure 2**) (17, 24, 42). Our data show discrete fitness patterns for the steps of  
136 beta-oxidation that appear to be largely dictated by chain length (**Figure 2**).



137  
138 **Figure 1: Cladogram correlation matrix of genome-wide fitness data of *P. putida* grown on fatty acids.** The  
139 matrix shows pairwise comparisons of Pearson correlations of fitness data from *P. putida* KT2440 RB-TnSeq  
140 libraries grown on fatty acids as well as glucose. The legend in top left shows Pearson correlation between two  
141 conditions with blue showing  $r = 1$ , and red showing  $r = 0$ . The conditions were tested in duplicate and the data  
142 from each are numbered (1 & 2).

143

144 When grown on fatty acids, many bacteria require the anaplerotic glyoxylate shunt to  
145 avoid depleting TCA cycle intermediates during essential biosynthetic processes. In *P. putida*,  
146 the two steps of the glyoxylate shunt are encoded by PP\_4116 (*aceA* - isocitrate lyase) and  
147 PP\_0356 (*glcB* - malate synthase). Transposon mutants in both of these genes showed serious  
148 fitness defects (fitness score < -3) when grown on nearly all of the fatty acids tested (**Figure 2**).  
149 However, the glyoxylate shunt genes appeared dispensable for growth on valerate (C5), and  
150 showed a more severe fitness defect when grown on heptanoate (C7). Complete beta-oxidation  
151 of valerate and heptanoate results in ratios of propionyl-CoA to acetyl-CoA of 1:1 and 1:2,  
152 respectively. This higher ratio of 3-carbon to 2-carbon production presumably offers an alternate  
153 means to replenish TCA cycle intermediates in the absence of a glyoxylate shunt (**Figure 2**).

154 In order to utilize the propionyl-CoA generated by beta-oxidation of odd-chain fatty  
155 acids, bacteria often employ the methylcitrate cycle (MCC), producing succinate and pyruvate  
156 from oxaloacetate and propionyl-CoA. In *P. putida*, the MCC is catalyzed via methylcitrate  
157 synthase (*prpC* - PP\_2335), 2-methylcitrate dehydratase (*prpD* - PP\_2338, or *acnB* - PP\_2339),  
158 aconitate hydratase (*acnB* - PP\_2339, or *acnA2* - PP\_2336), and 2-methylisocitrate lyase (*mmgF*  
159 - PP\_2334) (**Supplementary Figure 1**). Unsurprisingly, the MCC appeared to be absolutely  
160 required for growth on propionate (C3), valerate (C5), heptanoate (C7), and nonanoate (C9),  
161 with PP\_2334, PP\_2335, and PP\_2337 (a putative AcnD-accessory protein) showing severe  
162 fitness defects (**Figure 2, Supplementary Figure 1**). While PP\_2338 (*prpD*) encodes for a 2-  
163 methylcitrate dehydratase, transposon mutants showed no fitness defects when grown on odd-  
164 chain fatty acids. This reaction is likely carried out by PP\_2339 (*acnB* - a bifunctional 2-  
165 methylcitrate dehydratase/conitase hydratase B); however, there were no mapped transposon  
166 insertions for this gene (**Figure 2, Supplementary Figure 1**). This suggests that PP\_2339 was

167 essential during the construction of the RB-TnSeq library. Furthermore, PP\_2336 showed  
168 relatively modest fitness defects when grown on propionate and other odd-chain fatty acids,  
169 suggesting that PP\_2339 likely accounts for much of the methylaconitate hydratase activity as  
170 well (**Figure 2, Supplementary Figure 1**).

171

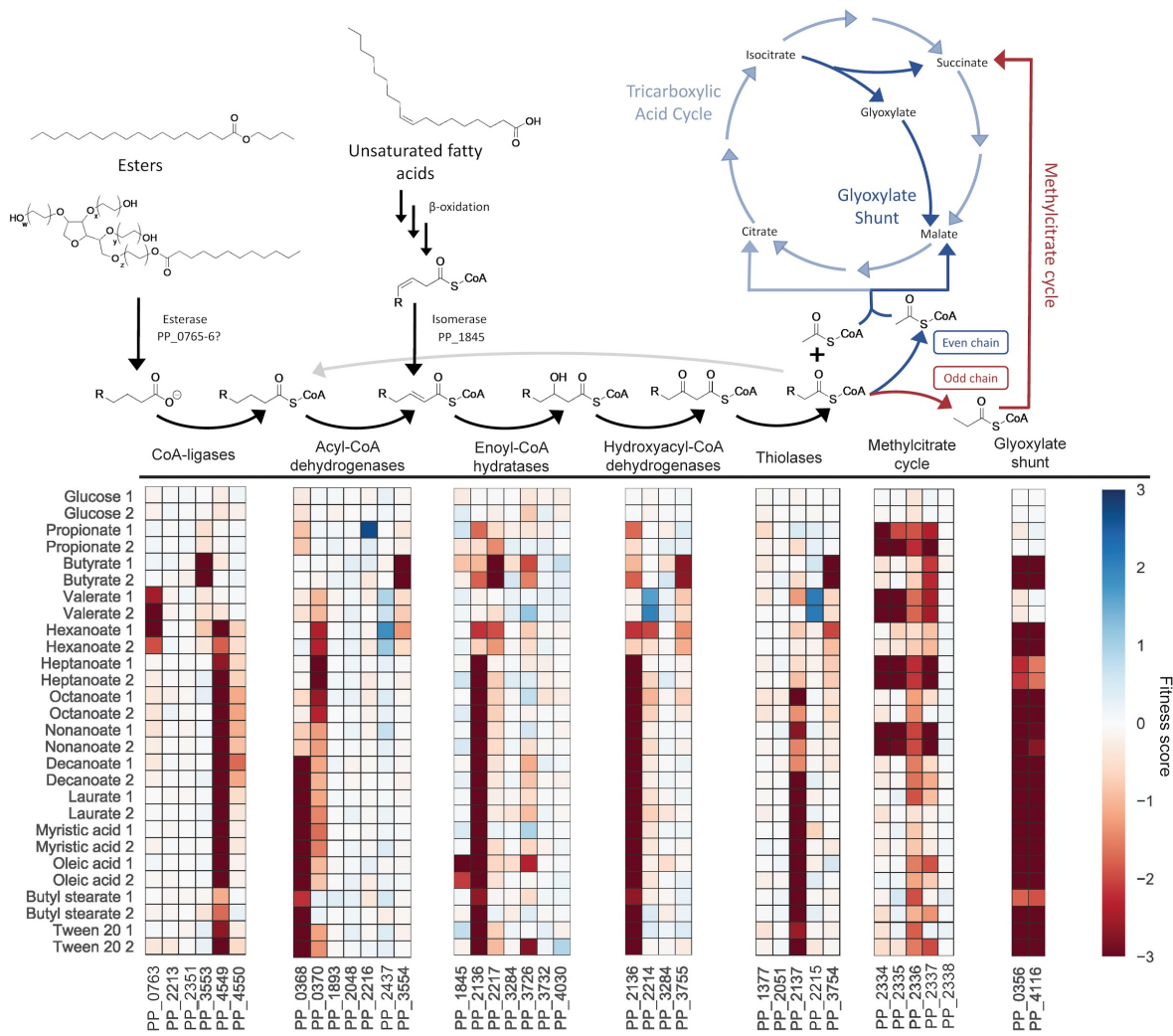
172 Long and Medium Chain Fatty Acid Catabolism. Pearson correlation analysis of fitness data  
173 indicated that both long and medium chain fatty acids are likely catabolized via similar  
174 pathways. Fitness data suggests that FadD1 (PP\_4549) catalyzes the initial CoA-ligation of C7 to  
175 C18 fatty acids, and may potentially act on C6 as well (**Figure 2**). Disruption of *fadD2*  
176 (PP\_4550) did not cause fitness defects as severe as those seen in *fadD1* mutants, although it did  
177 result in moderate fitness defects when grown on C8-C10 fatty acids. These data are consistent  
178 with the biochemical characterization of FadD1 from *P. putida* CA-3, which showed greater  
179 activity on longer chain alcanoic and phenylalkanoic acids than on shorter chain substrates (43).  
180 For fatty acids with chain lengths of C10 and greater, the data suggest that the *fadE* homolog  
181 PP\_0368 is the primary acyl-coA dehydrogenase, while the nearby *fadE* homolog PP\_0370  
182 appears to be preferred for C6-C8 fatty acids (**Figure 2**). A relatively even fitness defect for  
183 these two *fadE* homologs indicates that PP\_0368 and PP\_0370 may have equal activity on  
184 nonanoate (**Figure 2**). These data are supported by a previous biochemical characterization of  
185 PP\_0368, in which it showed greater activity on chain lengths longer than C9 (44). The *fadB*  
186 homolog PP\_2136 showed severe fitness defects when grown on all fatty acids with chain  
187 lengths of C6 and longer, implicating it as the primary enoyl-CoA hydratase/3-hydroxy-CoA  
188 dehydrogenase for those substrates (**Figure 2**). *P. putida* was able to grow on the unsaturated  
189 substrate oleic acid, and is likely able to isomerize the position of the unsaturated bond via the

190 enoyl-CoA isomerase PP\_1845, which showed specific fitness defects when grown on oleic acid  
191 (**Figure 2**). *P. putida*'s primary long chain thiolase appears to be the *fadA* homolog PP\_2137,  
192 which showed severe to moderate fitness defects when grown on fatty acids with chain lengths  
193 C8 or longer (**Figure 2**). Fitness data for mutant pools grown on heptanoate showed minor  
194 fitness defects for both PP\_2137 and PP\_3754 (*bktB*), suggesting that both thiolases may work  
195 on C7 substrates (**Figure 2**).

196 Both long chain fatty esters tested (Tween 20 and butyl stearate) appeared to utilize the  
197 same *fad* homologs as the long chain fatty acids. However, before either molecule can be  
198 directed towards beta-oxidation, Tween 20 and butyl stearate must be hydrolyzed to generate a  
199 C12 or C18 fatty acid, respectively. To date, no such hydrolase has been identified in *P. putida*  
200 KT2440. Comparing the mutant fitness scores between Tween 20 and laurate (C12) carbon  
201 source experiments revealed six genes (PP\_0765, PP\_0766, PP\_0767, PP\_0914, PP\_2018, and  
202 PP\_2019) that had significant and severe fitness defects specific to Tween 20 (fitness score < -2,  
203  $t > |4|$ ) in both biological replicates (**Figure S2**). The same comparison between butyl stearate  
204 and myristate (C14) revealed four genes specific to the fatty ester (PP\_0765, PP\_0766, PP\_2018,  
205 and PP\_4058) that had significant severe fitness defects (fitness score < -2,  $t > |4|$ ) in both  
206 biological replicates (**Figure S2**). As PP\_0765-6 and PP\_2018 appear to have specific  
207 importance in both of the ester conditions tested, it may be possible that they contribute to the  
208 hydrolysis of the fatty ester bonds. However, it is also possible that the esterase is secreted or  
209 associated with the outer membrane (45), in which case its enzymatic activity would be shared  
210 amongst the library and it would not have the associated fitness defect expected (10).

211 The genes PP\_2018 and PP\_2019 encode a BNR-domain containing protein and a RND-  
212 family efflux transporter, respectively, and are likely co-expressed in an operon that also

213 includes PP\_2020 and PP\_2021. Interestingly, although PP\_2021 codes for a putative lactonase,  
214 transposon mutants had no apparent fitness defect with either of the fatty esters as the carbon  
215 source. PP\_0765 and PP\_0766 encode a DUF1302 family protein and DUF1329 family protein,  
216 respectively. Given their similar fitness scores, they are likely coexpressed in an operon  
217 positively regulated by the LuxR-type regulator PP\_0767 (**Figure S2**). Previous work in multiple  
218 other species of *Pseudomonas* has observed cofitness of DUF1302/DUF1329 family genes with  
219 BNR-domain and RND-family efflux genes when grown on Tween 20 (41). The authors  
220 proposed that these genes may work together in order to export a component of the cell wall.  
221 However, an alternative hypothesis could be that PP\_0765 and PP\_0766 contribute to catalyzing  
222 the hydrolysis of fatty esters, accounting for the missing catabolic step of butyl stearate and  
223 Tween 20. This hypothesis is bolstered somewhat by the co-localization of PP\_0765/PP\_0766  
224 near fatty acid catabolic genes in *P. putida* KT2440 and many other *Pseudomonads* (**Figure S3**).  
225 Future work will need to be done to biochemically characterize the potential enzymatic activity  
226 of these proteins.



227

228 **Figure 2: Overview of fatty acid catabolic pathways of *P. putida* KT2440.** The above diagram shows the  
 229 catabolic steps of fatty ester and saturated/unsaturated fatty acid catabolism in *P. putida* KT2440, in addition to their  
 230 connections to the glyoxylate shunt and the methylcitrate cycle. The heatmaps below show fitness scores when  
 231 grown on fatty acids or glucose for the specific genes proposed to catalyze individual chemical reactions. Colors  
 232 represent fitness scores, with blue representing positive fitness and red representing negative fitness.

233

234

235

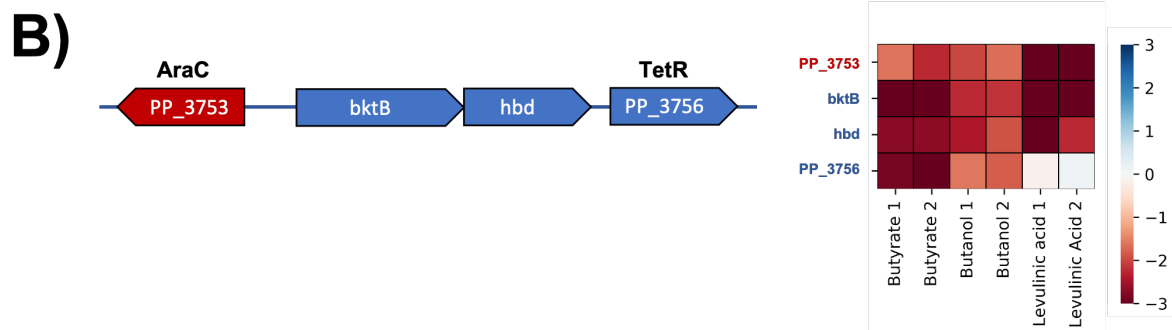
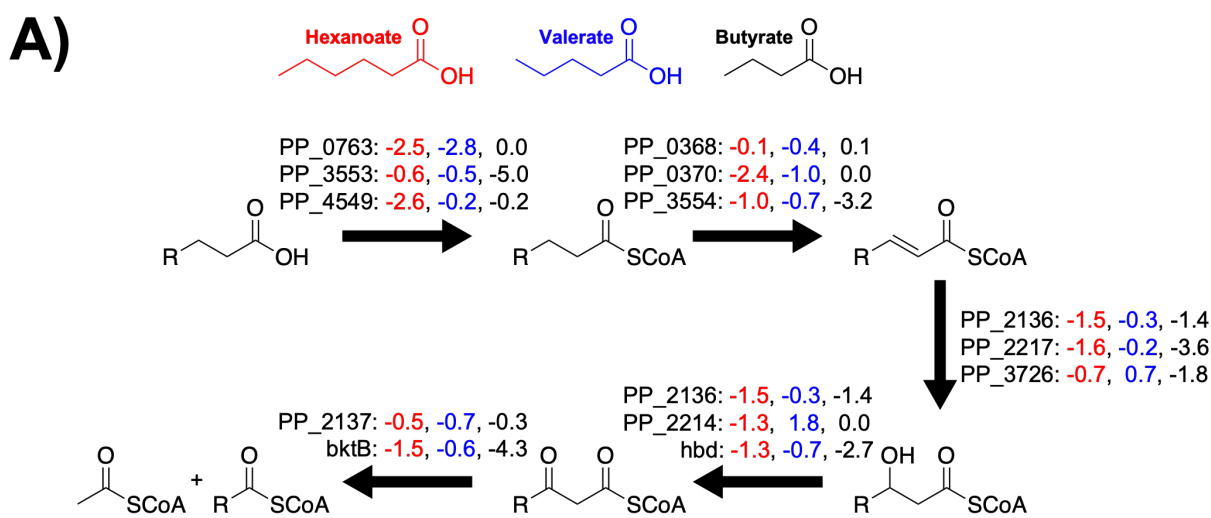
236

237 Short Chain Fatty Acid Catabolism.

238 In our genome-wide fitness assays, the mutant fitness patterns of C6 or shorter fatty acid  
239 carbon sources had lower Pearson correlation between one another than the correlations within  
240 long and medium-chain fatty acids (**Figure 1**). These global differences reflect what appear to be  
241 discrete preferences in beta-oxidation enzymes for growth on short chain fatty acids. Fitness data  
242 suggest that while both CoA-ligases PP\_0763 and PP\_4559 are required for growth on  
243 hexanoate, only PP\_0763 is required for growth on valerate (**Figure 2**). Furthermore, the  
244 putative positive regulator of PP\_0763, LuxR-family transcription factor PP\_0767, also showed  
245 a significant fitness defect (-2.0) when grown on both valerate and hexanoate (**Figure 2**).  
246 PP\_0370 seems to be the acyl-CoA dehydrogenase largely responsible for hexanoate catabolism,  
247 though PP\_3554 mutants also have minor fitness defects. The dehydrogenation of valeryl-coA  
248 appears to be distributed between the activities of PP\_0368, PP\_0370, and PP\_3554, with no  
249 single acyl-CoA dehydrogenase mutant demonstrating a strong fitness defect when grown on  
250 valerate (**Figure 2**). Interestingly, though previous biochemical analysis had demonstrated that  
251 PP\_2216 has activity on C4-C8 acyl-CoA substrates with a preference for shorter chain lengths  
252 (46), we observed no fitness defects for PP\_2216 mutants when grown on any fatty acid carbon  
253 source (**Figure 2**).

254 It appears that the role of enoyl-CoA hydratase or hydroxyacyl-CoA dehydrogenase may  
255 be distributed across multiple enzymes for both hexanoate and valerate. Growth on hexanoate  
256 resulted in moderate fitness defects in mutants disrupted in the predicted enoyl-CoA hydratases  
257 PP\_2136, PP\_2217, and PP\_3726; however, for mutants grown on valerate, there were almost no  
258 observable fitness defects for any of the enoyl-CoA hydratase enzymes examined in the study,  
259 suggesting that for this chain length significant functional complementation exists between the

260 *fadB* homologs (**Figure 2**). Fitness data suggest that PP\_2136 (*fadB*), PP\_2214 (a predicted type  
261 II 3-hydroxyacyl-CoA dehydrogenase), and PP\_3755 (a 3-hydroxybutyryl-CoA dehydrogenase)  
262 may all be involved in the dehydrogenation of 3-hydroxyhexanoyl-CoA (**Figure 2**), while there  
263 appears to be a distribution of *fadB*-like activity when it comes to the dehydrogenation of 3-  
264 hydroxyvaleryl-CoA, with PP\_3755 showing only a slight fitness defect on valerate.  
265 Intriguingly, mutants disrupted in the predicted type-2 acyl-CoA dehydrogenase PP\_2214  
266 showed apparent increased fitness when grown on valerate (**Figure 2**). As with heptanoate,  
267 fitness data from mutant pools grown on valerate or hexanoate suggest that both PP\_2137 and  
268 PP\_3754 may catalyze the terminal thiolase activity of these substrates. The lack of pronounced  
269 fitness phenotypes for the beta-oxidation steps of both valerate and hexanoate underscores the  
270 necessity for further *in vitro* biochemical interrogation of these pathways.



271

272 **Figure 3: Putative pathways for short chain fatty acid catabolism in *P. putida* KT2440.** A) Individual enzymatic  
273 steps that potentially catalyze the steps of beta-oxidation for short chain fatty acids, fitness scores are listed to the  
274 right of each enzyme when grown on either butyrate, valerate, or hexanoate. B) The operonic structure of *btkB* and  
275 *hdb* flanked by an AraC-family (PP\_3753) and TetR-family (PP\_3756). The heatmap shows fitness scores of the  
276 genes when grown on butyrate, butanol, or levulinic acid.

277

278 Both the butanol and butyrate metabolism of *P. putida* have been studied in detail  
279 through omics-level interrogation across multiple strains (28, 29). Previous work showed that  
280 during growth on n-butanol, which is later oxidized to butyrate, three CoA-ligases are up-  
281 regulated: PP\_0763, PP\_3553, and PP\_4487 (*acsA-1* - an acyl-CoA synthase) (29). However, our  
282 butyrate carbon source experiments only revealed strong fitness defects in PP\_3553 mutants  
283 (**Figure 2, Figure 3A**). The same work found that PP\_3554 was the only upregulated acyl-CoA  
284 dehydrogenase, which agrees with the strong fitness defect we observed in mutants of that gene  
285 (29). That prior work did not find upregulation of any enoyl-CoA hydratase in *P. putida* grown  
286 on butanol, but this is likely reflective of redundancy in this step; we observed fitness defects in  
287 multiple genes, including PP\_2136, PP\_2217, and PP\_3726, with mutants in PP\_2217  
288 demonstrating the most severe fitness defect (**Figure 2, Figure 3A**). Hydroxyacyl-CoA  
289 dehydrogenase PP\_2136 and 3-hydroxybutyryl-CoA dehydrogenase PP\_3755 (*hdb*) have both  
290 been shown to be upregulated during growth on butanol (29). While our data showed fitness  
291 defects in both of these genes, the defect of PP\_3755 mutants was much more severe. Three  
292 different thiolases (PP\_2215, PP\_3754, and PP\_4636) and the 3-oxoacid CoA-transferase *atoAB*  
293 were previously observed to be upregulated during growth on butanol, but of these genes, only  
294 PP\_3754 (*btkB*) had a strong fitness defect, implying that it is the main thiolase for the terminal  
295 step of butyrate catabolism (**Figure 2, Figure 3A**).

296                   The inability of the RB-TnSeq data to clearly show which enzymes are likely responsible  
297                   for specific beta-oxidation reactions suggest multiple enzymes may catalyze these steps. In  
298                   addition to the lack of genotype to phenotype clarity in the enzymes responsible for the catabolic  
299                   steps, we observed additional phenotypes within our fitness data that portray a complex picture  
300                   of short chain fatty acid metabolism in *P. putida*. The TetR-family repressor *paaX* (PP\_3286)  
301                   was shown to have a negative fitness score when mutant pools were grown on fatty acids with  
302                   chain lengths C7 or below (**Figure S4**). PaaX negatively regulates the *paa* gene cluster encoding  
303                   the catabolic pathway for phenylalanine (47, 48), implying that presence of phenylalanine  
304                   catabolism impedes growth on short chain fatty acids. It is therefore somewhat surprising that no  
305                   individual mutant within the *paa* gene cluster shows a fitness increase when grown on short  
306                   chain fatty acids, though no robust fitness data exists for *paaJ* (PP\_3275 - a 3-oxo-5,6-  
307                   didehydrosoberyl-coA thiolase) (**Figure S4**).

308                   Mutants in MerR-family regulator PP\_3539 showed very high fitness benefits (fitness  
309                   scores of 3.8 and 4.7 in two biological replicates) when grown on valerate. PP\_3539 likely  
310                   increases expression of *mvaB* (PP\_3540 - hydroxymethyl-glutaryl-CoA lyase), thus suggesting  
311                   that decreased levels of MvaB activity may benefit *P. putida* valerate catabolism. Unfortunately,  
312                   there are no fitness data available for *mvaB*, likely because it is essential under the conditions in  
313                   which the initial transposon library was constructed. The genes *hdb* and *bktB*, encoding the  
314                   terminal two steps of butyrate metabolism, are flanked upstream by an AraC-family regulator  
315                   (PP\_3753) and downstream by a TetR-family regulator (PP\_3756); the latter is likely co-  
316                   transcribed with the butyrate catabolic genes (**Figure 3B**). When grown on butyrate, mutants in  
317                   both PP\_3753 and PP\_3756 show decreased fitness; however, previous work to evaluate global  
318                   fitness of *P. putida* grown on levulinic acid showed negative fitness values only for PP\_3753,

319 *htb*, and *btkB* (**Figure 3B**). These results suggest that the TetR repressor may be responding to a  
320 butyrate specific metabolite. Finally, across multiple fitness experiments, the TonB siderophore  
321 receptor PP\_4994 and the TolQ siderophore transporter PP\_1898 showed fitness advantages  
322 when grown on fatty acids, especially on hexanoate (**Figure S5**). Together, these results suggest  
323 that a wide range of environmental signals impact how *P. putida* is able to metabolize short  
324 chain fatty acids.

325

326 **Global Analysis of Alcohol Catabolism**

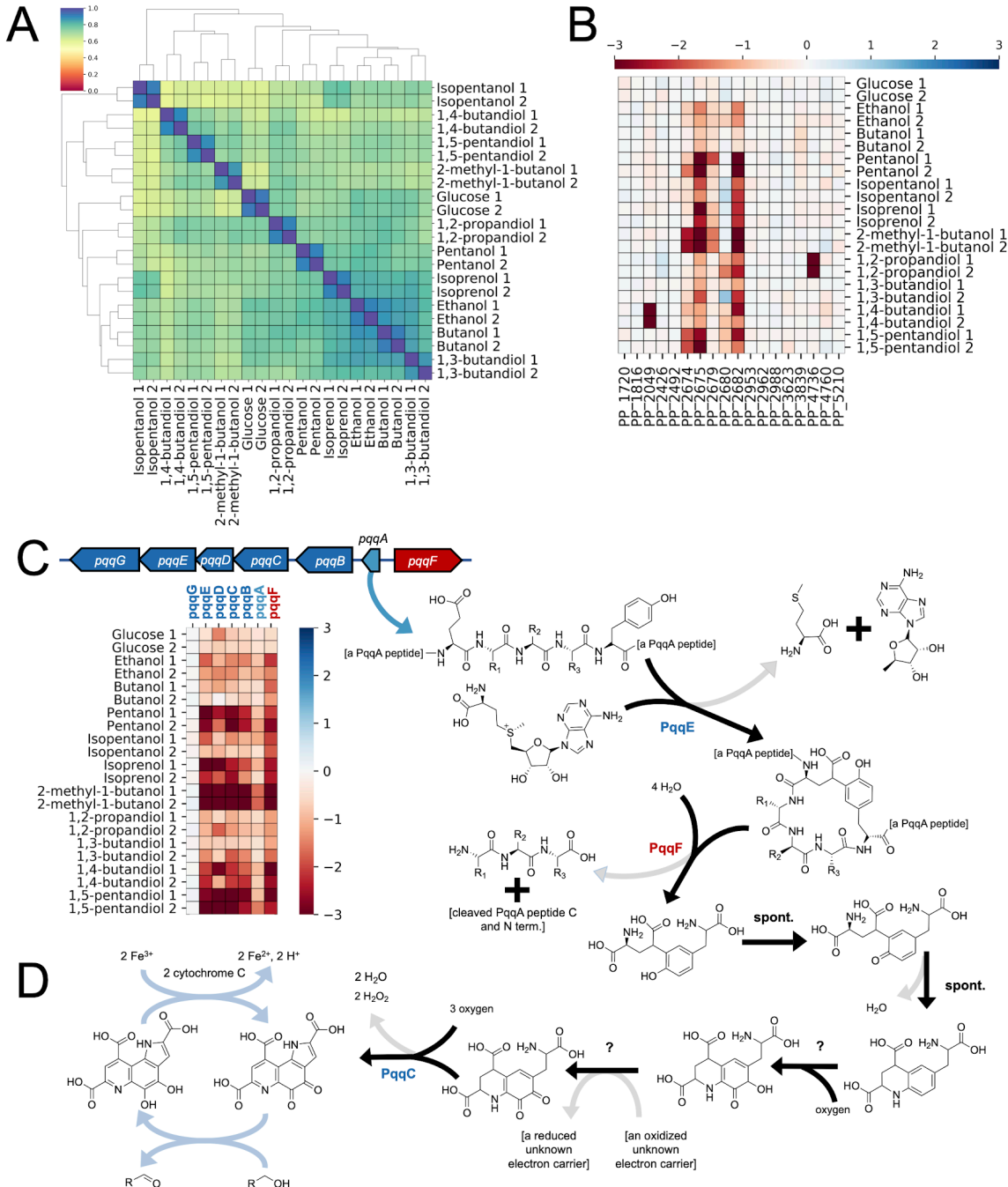
327 In addition to its ability to robustly catabolize a wide range of fatty acid substrates, *P.*  
328 *putida* is also capable of oxidizing and catabolizing a wide variety of alcohols into central  
329 metabolism through distinct pathways. To further our understanding of these pathways,  
330 transposon libraries were grown on a number of short n-alcohols (ethanol, butanol, and  
331 pentanol), diols (1,2-propanediol, 1,3-butanediol, 1,4-butanediol, and 1,5-pentanediol), and  
332 branched chain alcohols (isopentanol, isoprenol, and 2-methyl-1-butanol). Relative to growth on  
333 fatty acids, fitness experiments of *P. putida* grown on various alcohols showed less correlation to  
334 one another, reflecting the more diverse metabolic pathways used for their catabolism (**Figure**  
335 **4A**). The initial step of the catabolism of many primary alcohols is the oxidation of the alcohol to  
336 its corresponding carboxylic acid. The BioCyc database features 14 genes annotated as alcohol  
337 dehydrogenases (PP\_1720, PP\_1816, PP\_2049, PP\_2492, PP\_2674, PP\_2679, PP\_2682,  
338 PP\_2827, PP\_2953, PP\_2962, PP\_2988, PP\_3839, PP\_4760, and PP\_5210) (24). Fitness data  
339 showed that the majority of these alcohol dehydrogenases had no fitness defects when grown on  
340 the alcohols used in this study (**Figure 4B**).

341                   The alcohol dehydrogenases that showed the most consistent fitness defects across  
342                   multiple conditions were the two PQQ-dependent alcohol dehydrogenases PP\_2674 (*pedE*) and  
343                   PP\_2679 (*pedH*), as well as the Fe-dependent alcohol dehydrogenase PP\_2682 (*yiaY*) (**Figure**  
344                   **4B**). Both *pedE* and *pedH* have been extensively studied in *P. putida* and other related bacteria,  
345                   and are known to have broad substrate specificities for alcohols and aldehydes (25, 26, 49). Their  
346                   activity is dependent on the activity of *pedF* (PP\_2675), a cytochrome *c* oxidase that regenerates  
347                   the PQQ cofactor (25). In *P. aeruginosa*, a homolog of *yiaY* (*ercA*) was shown to have a  
348                   regulatory role in the expression of the *ped* cluster, and was not believed to play a direct  
349                   catabolic role (50). In most conditions tested, disruption of *pedF* caused more severe fitness  
350                   defects than either *pedE* or *pedH* individually, suggesting they can functionally complement one  
351                   another in many cases. However, growth on 2-methyl-1-butanol and 1,5-pentanediol both  
352                   showed more severe fitness defects in *pedE* mutants compared to *pedF* (**Figure 4B**). In many  
353                   other alcohols, including ethanol and butanol, even disruption of *pedF* did not cause extreme  
354                   fitness defects, suggesting the presence of other dehydrogenases able to catalyze the oxidation  
355                   (**Figure 4B**).

356                   The transcriptional regulatory systems that activate expression of various genes in the *ped*  
357                   cluster could also be identified from these data. Mutants in either member of the sensory  
358                   histidine kinase/response regulator (HK/RR) two component system, *pedS2/pedR2*, showed  
359                   significant fitness defects when 2-methyl-1-butanol was supplied as the sole carbon source. This  
360                   HK/RR signaling system has been shown to activate the transcription of *pedE* and repress *pedH*  
361                   in the absence of lanthanide ions (51). Since lanthanides were not supplied in the medium, this  
362                   likely explains the fitness defect observed in *pedS2/pedR2*. The transcription factor *pedR1*  
363                   (*agmR*) was also found to affect host fitness when grown on various alcohols (**Figure 5**). This

364 gene has been identified in *P. putida* U as an activator of long chain (C6+) n-alcohol and  
365 phenylethanol catabolism (52). In *P. putida* KT2440, *pedR1* has been associated with the host  
366 response to chloramphenicol, and its regulon has been elucidated previously (53). Our data  
367 reflect the literature, indicating that *pedR1* functions as a transcriptional activator of the *ped*  
368 cluster and *pedR2* functions as a specific regulator of *pedE* and *pedH*.

369 Unsurprisingly, the genes required for the biosynthesis of the PQQ cofactor were also  
370 amongst the most co-fit (cofitness is defined as Pearson correlation between fitness scores of two  
371 genes over many independent experimental conditions) with both *pedF* and *yiaY*. *P. putida*  
372 synthesizes PQQ via a well-characterized pathway, starting with a peptide encoded by the gene  
373 *pqqA* (PP\_0380) which is then processed by *pqqE*, *pqqF*, and *pqqC* to generate the final cofactor  
374 (**Figure 4C**). The three synthetic genes (*pqqEFC*) all showed significant fitness defects on the  
375 same alcohols as the *pedF* mutants, while *pqqA* showed a less severe fitness phenotype (**Figure**  
376 **4C**). However, the small size of *pqqA* resulted in few transposon insertions, making it difficult to  
377 draw confident conclusions. Two genes showed similar defective fitness patterns on select  
378 alcohols: *pqqB*, which has been proposed to be an oxidoreductase involved in PQQ biosynthesis;  
379 and *pqqD*, a putative PQQ carrier protein. Previous work regarding a PqqG homolog from  
380 *Methylorubrum extorquens* suggested that it forms a heterodimeric complex with PqqF that  
381 proteolytically processes PqqA peptides, although PqqF was sufficient to degrade PqqA on its  
382 own (54). Fitness data from *P. putida* may support this hypothesis, as there was no observed  
383 fitness defect in *pqqG* mutants when grown on any alcohol, suggesting that the bacterium is still  
384 able to process PqqA with PqqF alone (**Figure 4C**).



386 **Figure 4: Global analysis of alcohol metabolism in *P. putida*.** A) Pairwise comparisons of Pearson correlations of  
387 fitness data from *P. putida* KT2440 RB-TnSeq libraries grown on alcohols as well as glucose grouped by overall  
388 similarity. Colors bar at top left shows the Pearson coefficient with 1 indicating greater similarity and 0 indicating  
389 greater dissimilarity. B) Heatmap shows the fitness scores of all alcohol dehydrogenases annotated on the BioCyc  
390 database as well as the cytochrome C PP\_2675 when grown on various alcohols and glucose. C) Operonic diagram  
391 of the *pqq* cluster in *P. putida* and the corresponding biosynthetic pathway for the PQQ cofactor and D) How PQQ  
392 cofactors are regenerated by cytochrome C. Heatmap shows fitness scores for individual *pqq* cluster genes when  
393 grown on alcohols and glucose.

394

395

396

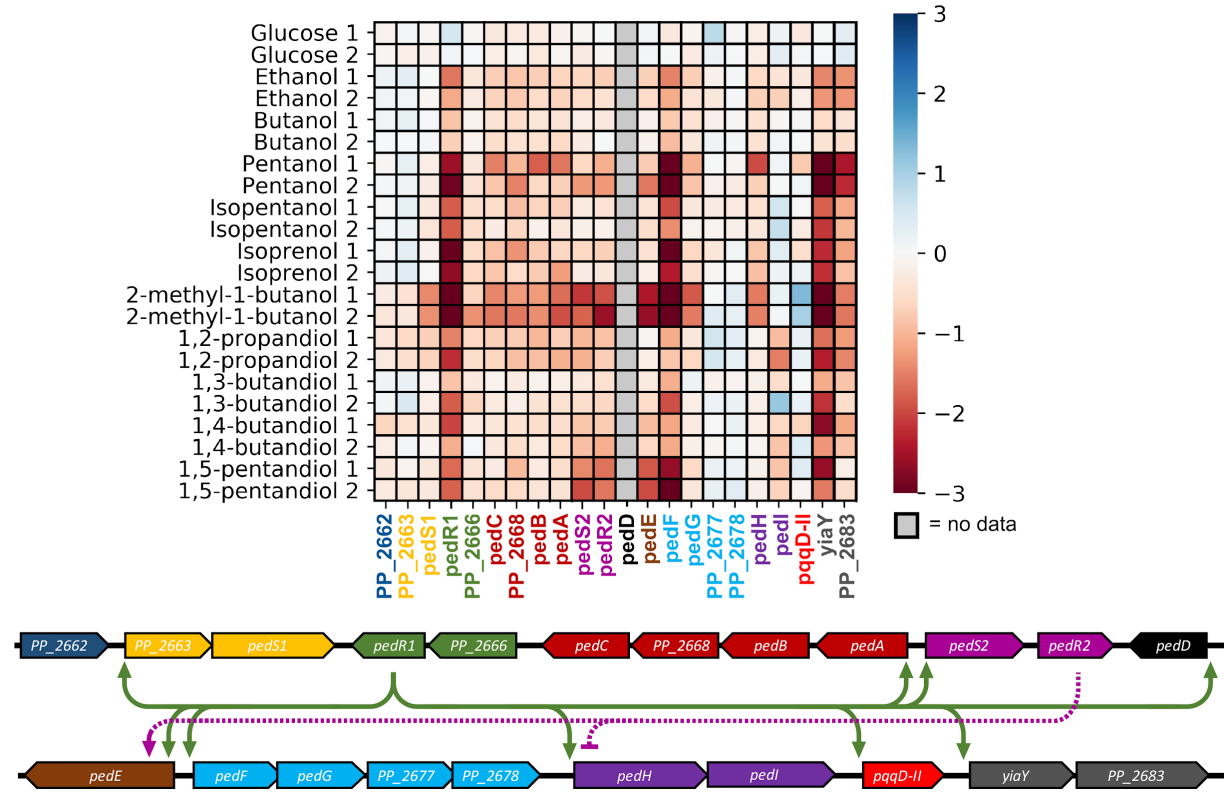
397

398

399

400

401



403 **Figure 5: Essentiality and regulation of the *ped* cluster.** (Top) Heatmap depicting the fitness scores for genes in  
 404 the *ped* cluster (PP\_2662 to PP\_2683) during growth on various short chain alcohols. (Bottom) Genomic context for  
 405 the *ped* cluster in *P. putida* KT2440. Arrows depict transcriptionally upregulated genes of *pedR1* and *pedR2*. Blunt  
 406 arrows point to genes predicted to be transcriptionally repressed in the condition tested.

407 Short chain alcohol metabolism

408 The metabolism of n-alcohols almost certainly proceeds through beta-oxidation using the  
 409 same enzymatic complement as their fatty acid counterparts. This relationship is reflected in the  
 410 high correlation in global fitness data between alcohols and fatty acids of the same chain length  
 411 (ethanol and acetate -  $r = 0.72$ , butanol and butyrate -  $r = 0.66$ , pentanol and valerate -  $r = 0.72$ ).  
 412 However, given previous work and our fitness data, the initial oxidation of these alcohols

413 appears to be quite complex. Biochemical characterization of both PedE and PedH have shown  
414 that both have activity on ethanol, acetaldehyde, butanol, butyraldehyde, hexanol, and  
415 hexaldehyde (25). When grown on n-pentanol, mutants disrupted in *pedF* show severe fitness  
416 defects, suggesting that PedH and PedE are the primary dehydrogenases responsible for pentanol  
417 oxidation (**Figure 4B**, **Figure 5A**). However, when grown on either ethanol or n-butanol, both  
418 the PQQ-dependent alcohol dehydrogenases (PQQ-ADHs) and *pedF* show less severe fitness  
419 defects compared to when they are grown on pentanol (**Figure 4B**). This implies that other  
420 dehydrogenases are also capable of these oxidations. One likely candidate may be PP\_3839,  
421 which shows a minor fitness defect when grown on n-butanol and has been biochemically shown  
422 to oxidize coniferyl alcohol (**Figure 4B**) (55). Individual gene deletion mutants of either *pedF*  
423 (PP\_2675) or PP\_3839 showed only minor growth defects when grown on either ethanol,  
424 butanol, or pentanol as a sole carbon source (**Figure 7**). However, when both genes were deleted,  
425 no growth was observed on these substrates, suggesting that the PQQ-ADHs and PP\_3839 are  
426 the primary dehydrogenases responsible for the oxidation of short chain n-alcohols (**Figure 7**).

427 It is ambiguous from our data and from previous work which enzymes are oxidizing the  
428 aldehyde to the corresponding carboxylic acid. As mentioned previously, both PQQ-ADHs have  
429 been biochemically shown to act on aldehydes and could catalyze the reaction, but the lack of a  
430 strong fitness phenotype for both ethanol and n-butanol suggest they are not the only enzymes  
431 capable of catalyzing this reaction. The genomically proximal aldehyde dehydrogenase *pedI*  
432 (PP\_2680) showed minor fitness defects when grown on ethanol and several other alcohols  
433 (**Figure 5**, **Figure 6A**), but showed no fitness defects when libraries were grown on butanol or  
434 pentanol. Another aldehyde dehydrogenase, *aldB-I* (PP\_0545), showed virtually no fitness  
435 defects when grown on any of the short chain n-alcohols tested here (**Figure 6A**). The lack of

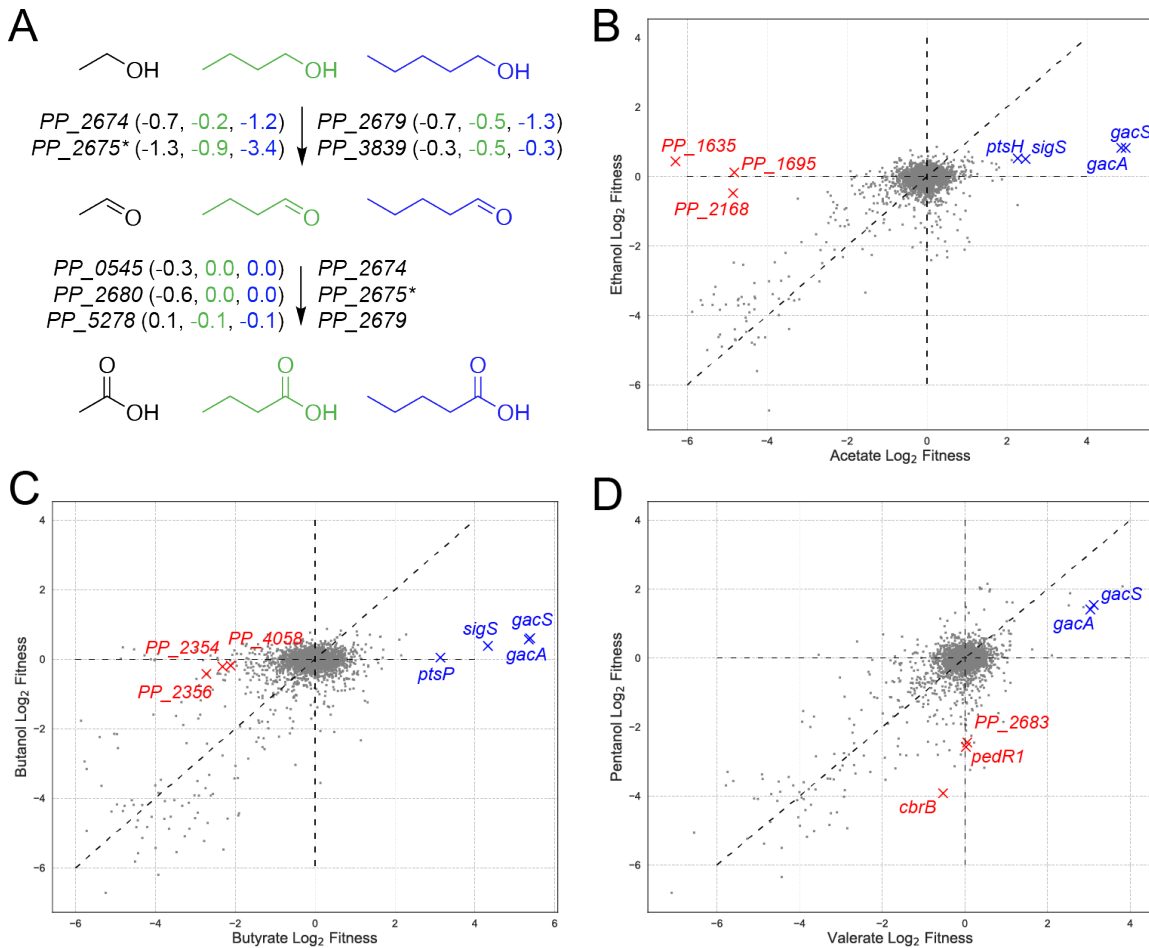
436 any one obvious enzyme with a distinct fitness defect supports the notion that multiple enzymes  
437 are present and able to catalyze the oxidation of these aldehydes.

438 While the metabolism of alcohols and their corresponding fatty acids are similar, their  
439 fitness patterns showed distinct differences. When grown on acetate, mutants in *gacS* or *gacA*  
440 (PP\_1650 and PP\_4099 - a two-component (TCS) system), *sigS* (PP\_1623 - the stationary phase  
441 sigma factor sigma S), and *ptsH* (PP\_0948 - a component of the sugar phosphotransferase system  
442 (PTS)) showed large and significant fitness benefits, which were not apparent when grown on  
443 ethanol (**Figure 5B**). The GacS/GacA TCS is widespread across many gram-negative bacteria,  
444 and is believed to exert transcriptional control over a wide variety of functions, sometimes in  
445 concert with a small RNA binding protein (CsrA) that exerts post-transcriptional control (56). In  
446 *Pseudomonads*, the GacA/GacS TCS has been implicated in positively controlling *sigS*  
447 expression in multiple species (57). In *P. putida* specifically, *gacS* mutations in strains  
448 engineered to produce muconic acid have resulted in higher titers (58), but disruption of the gene  
449 was also shown to completely abolish production of medium-chain length  
450 polyhydroxyalkanoates (PHAs) (59). Growth on butyrate also showed that *gacS*, *gacR*, *sigS*, and  
451 another component of the PTS (*ptsP*) had significant fitness benefits if disrupted, which was not  
452 observed when the library was grown on butanol (**Figure 5C**). Interestingly, mutants in *gacA* and  
453 *gacS* seemed to have fitness benefits when grown on either pentanol or valerate (**Figure 5D**).  
454 Further work is necessary to precisely characterize the nature of the benefits that occur when  
455 these genes are disrupted.

456 When grown on ethanol compared to acetate, relatively few genes not involved in the  
457 oxidation of the short chain alcohols were found to be specifically and significantly unfit;  
458 however, specific phenotypes for acetate catabolism were observed (**Figure 5B**). Mutants in

459 PP\_1635 (a two-component system response regulator), PP\_1695 (variously annotated as a  
460 sodium-solute symporter, sensory box histidine kinase, or response regulator), and *tal* (PP\_2168  
461 - transaldolase) all showed fitness defects on acetate that were not observed when libraries were  
462 grown on ethanol. The high cofitness between PP\_1635 and PP\_1695 observed across all  
463 publicly available fitness data ( $r = 0.88$ ) and share homology to *crbSR* systems of other bacteria  
464 where it is known to regulate acetyl-coA synthetase (60).

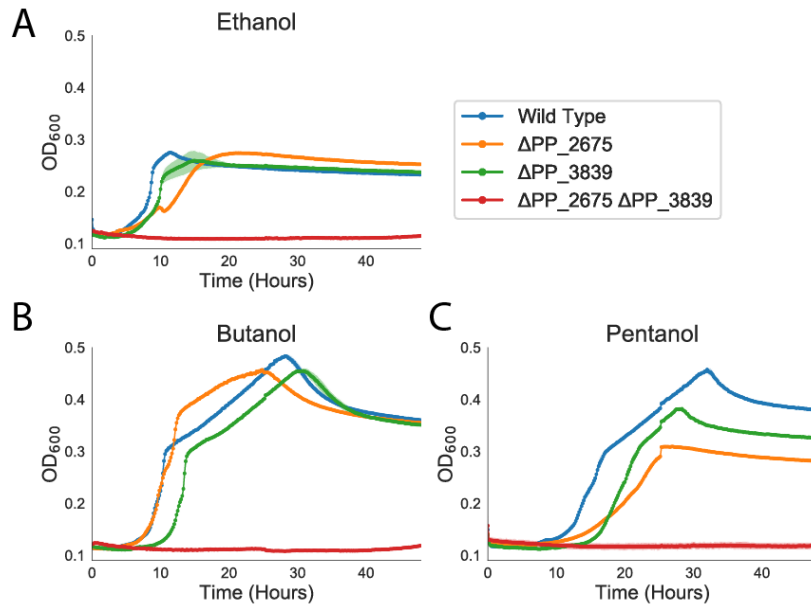
465 Much like ethanol and acetate, there were relatively few genes that showed specific  
466 fitness defects when grown on butanol that were not also observed in butyrate. However, the  
467 genes *glgB* (PP\_4058 - a 1,4-alpha-glucan branching enzyme), and the co-transcribed PP\_2354  
468 and PP\_2356 (annotated as a histidine kinase/response regulator (HK/RR), and histidine kinase  
469 respectively) showed specific fitness defects when grown on butyrate relative to butanol.  
470 PaperBLAST analysis of PP\_2356 and PP\_2354 did not reveal any publications that had  
471 explored the function of this system, and thus further work will be needed to better characterize  
472 its regulon (61). Mutants of genes encoding for three TCSs were found to be specifically unfit  
473 when grown on pentanol when compared to valerate. PP\_2683 (a two component HK/RR), and  
474 *pedR1* (PP\_2665 - RR) were both specifically unfit and, as previously described, are involved in  
475 the regulation of the *ped* cluster (**Figure 5D**). The gene *cbrB* (PP\_4696 - sig54-dependent RR)  
476 also showed pentanol-specific defects, and is known to regulate central carbon metabolism and  
477 amino acid uptake in the *Pseudomonads* (62, 63).



478

479 **Figure 6: Analysis of short chain alcohol metabolism in *P. putida*:** A) Putative genes involved in the initial  
480 oxidation steps of short chain alcohol assimilation in *P. putida*. PP\_2675 (PedF) is involved in the regeneration of  
481 the PQQ cofactor predicted to be necessary for these oxidation reactions of PP\_2764 (PedE) and PP\_2769 (PedH).  
482 Average fitness scores for two biological reps are shown next to each gene for ethanol (black), butanol (green), and  
483 pentanol (blue). Scatter plots show global fitness scores for ethanol versus acetate (B), butanol versus butyrate (C),  
484 and pentanol versus valerate (D).

485



486

487 **Figure 7: Validation of alcohol dehydrogenases involved in short chain alcohol metabolism** Growth curves of  
488 wild type (blue), ΔPP\_2675 (orange), ΔPP\_3839 (green), and ΔPP\_2675ΔPP\_3839 (red) strains of *P. putida*  
489 KT2440 on 10 mM ethanol (A), 10 mM n-butanol (B), and 10 mM n-pentanol (C). Shaded area represents 95%  
490 confidence intervals (cI), n=3.

491

492 Short chain diol catabolism

493 Another group of industrially relevant alcohols with potential for biotechnological  
494 production are short chain diols. These compounds have broad utility ranging from plasticizers to  
495 food additives (64). As shown in **Figure 5**, most of the tested short chain diols result in  
496 significant fitness defects in *pedR1*, indicating that some of the genes involved in these  
497 metabolisms are in the PedR1 regulon. However, only 1,5-pentanediol had a strong fitness defect  
498 in *pedF*, indicating that multiple dehydrogenases may act on the shorter chain diols.

499 Additionally, both 1,2-propanediol and 1,3-butanediol cause slight defects in mutants of the  
500 aldehyde dehydrogenase PP\_0545. Although there is some ambiguity as to which enzymes

501 initially oxidize the diols to their corresponding acids, the remaining steps in 1,2-propanediol,  
502 1,3-butanediol, and 1,5-pentanediol catabolism are much more straightforward.

503           Oxidation of 1,2-propanediol yields lactate, and mutants in the L-lactate permease  
504 PP\_4735 (*lldP*) have a fitness of -4.3 when grown on 1,2-propanediol. Furthermore, under this  
505 condition, mutants of the L- and D- lactate dehydrogenases PP\_4736 (*lldD*) and PP\_4737 (*lldE*)  
506 have fitness defects of -5.0 and -1.5, respectively. Since we provided a rac-1,2-propanediol as a  
507 substrate, this likely explains the fitness defects observed in both dehydrogenases (65, 66). Given  
508 these results, it appears that 1,2-propanediol is assimilated into central metabolism via oxidation  
509 to pyruvate (**Figure S6**).

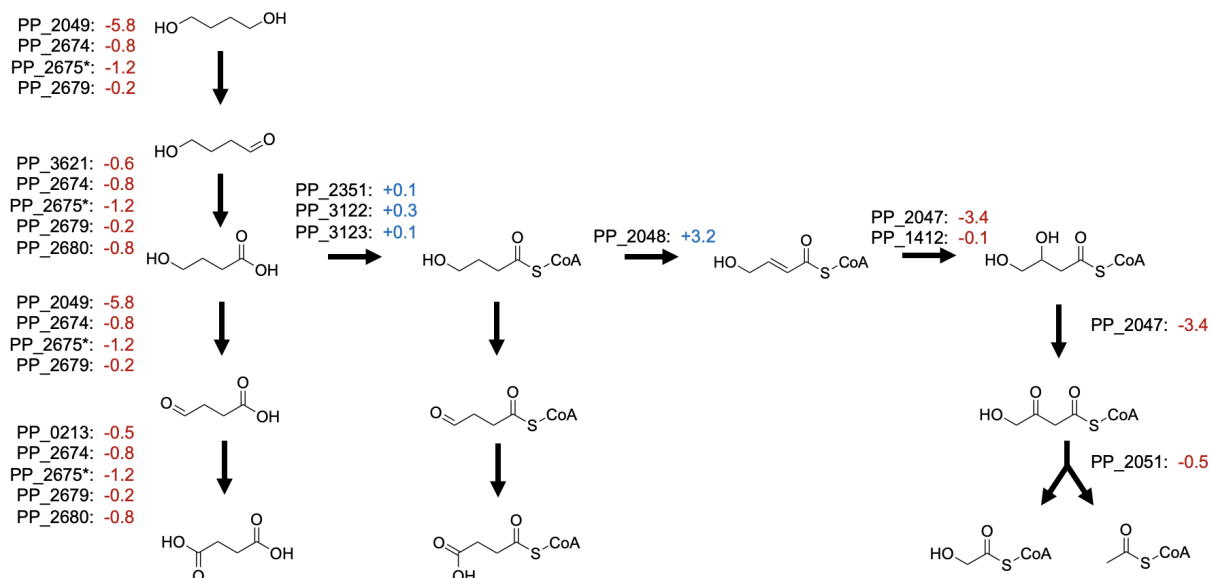
510           When grown on 1,3-butanediol, two oxidations of 1,3-butanediol result in 3-  
511 hydroxybutyrate, and we observe fitness defects of -2.5 in the D-3-hydroxybutyrate  
512 dehydrogenase PP\_3073 and -1.8 in the neighboring sigma-54 dependent regulator PP\_3075  
513 (67). Dehydrogenation of 3-hydroxybutyrate results in acetoacetate, and we see a fitness defect  
514 of -2.9 and -3.0 for the subunits of the predicted 3-oxoacyl-CoA transferase PP\_3122-3 (*atoAB*).  
515 This enzyme likely transfers a CoA from either succinyl-CoA or acetyl-CoA in order to generate  
516 acetoacetyl-CoA. Regarding transport, mutants in the D-beta-hydroxybutyrate permease  
517 PP\_3074, located in the same operon as the 3-hydroxybutyrate dehydrogenase, have a fitness  
518 defect of -0.9, while mutants in the RarD permease PP\_3776 have a fitness of -1.2.

519           Following oxidation by the aforementioned PQQ-dependent dehydrogenases and  
520 aldehyde dehydrogenases in the periplasm, an oxidized intermediate is likely transported into the  
521 cell for the next steps in the catabolism. This is supported by the observation that mutants of the  
522 predicted dicarboxylate MFS transporter PP\_1400 and its two-component regulator PP\_1401-2  
523 have strong fitness defects on both alpha-ketoglutarate and 1,5-pentanediol. Furthermore, there is

524 a -4.7 fitness defect in mutants of the L-2-hydroxyglutarate oxidase PP\_2910, which catalyzes  
525 the second step in the glutarate hydroxylation pathway of glutarate catabolism. The glutarate  
526 hydroxylase PP\_2909, which catalyzes the first step of this pathway, has a much slighter  
527 negative fitness of -0.6. This is expected, because glutarate can also be catabolized through a  
528 glutaryl-CoA dehydrogenation pathway, so mutants in PP\_2909 can simply divert flux through  
529 the other catabolic route (12). Mutants in PP\_2910 are unable to oxidize L-2-hydroxyglutarate to  
530 alpha-ketoglutarate, and likely accumulate L-2-hydroxyglutarate as a dead-end metabolite.

531 1,4-butanediol catabolism has been previously studied; based on the results of expression  
532 data and adaptive laboratory evolution, Li et al. proposed three potential catabolic pathways for  
533 1,4-butanediol, including a beta-oxidation pathway (**Figure 8**) (30). Their evolved strains had  
534 mutations in the LysR activator PP\_2046 that resulted in overexpression of the beta-oxidation  
535 operon PP\_2047-51 (30). Interestingly, we found that when grown on 1,4 butanediol, transposon  
536 mutants of the acyl-CoA dehydrogenase PP\_2048 had significant fitness benefits and no CoA-  
537 ligase mutants showed significant fitness defects. However, a fitness defect of -1.0 in PP\_0356  
538 (malate synthase) mutants suggests that there may be flux through the beta-oxidation pathway to  
539 glycolic acid and acetyl-CoA. A possible explanation for the positive fitness of PP\_2048 mutants  
540 is that the beta-oxidation pathway is suboptimal in the wild type, and it may be beneficial to  
541 divert flux through the other pathway(s). This same reasoning could also explain the absence of  
542 CoA-ligases with fitness defects; however, this also could be due to the presence of multiple  
543 CoA-ligases capable of catalyzing that step. Mutants of the 3-hydroxyacyl-CoA dehydrogenase  
544 PP\_2047, a *fadB* homolog which likely catalyzes the hydration and dehydrogenation steps to  
545 produce 3-oxo-4-hydroxybutyryl-CoA, had a strong fitness defect. When PP\_2047 is non-  
546 functional, 4-hydroxycrotonyl-CoA likely accumulates as a deadend metabolite resulting in

547 decreased fitness. Li et al. also showed that deletion mutants of PP\_2046 are unable to grow on  
548 1,4-butanediol (30). Our data suggests that this is because PP\_2049 appears to be the main  
549 alcohol dehydrogenase acting on either 1,4-butanediol or 4-hydroxybutyrate, and is in the operon  
550 under the control of PP\_2046. Although our fitness data suggests that both the oxidation to  
551 succinate and beta-oxidation pathways occur, further work is necessary to determine if the  
552 pathway to succinyl-CoA is involved in the catabolism.



554 **Figure 8: Putative routes of 1,4-butanediol catabolism in *P. putida*.** Putative genes involved in catabolism of 1,4-  
555 butanediol in *P. putida*. Average fitness scores for two biological reps are shown next to each gene. The three CoA-  
556 ligases shown were proposed by Li et al.; there were no CoA-ligases that showed significant fitness defects on 1,4-  
557 butanediol. \*PP\_2675 (PedF) is involved in the regeneration of the PQQ cofactor predicted to be necessary for these  
558 oxidation reactions of PP\_2764 (PedE) and PP\_2769 (PedH).

559

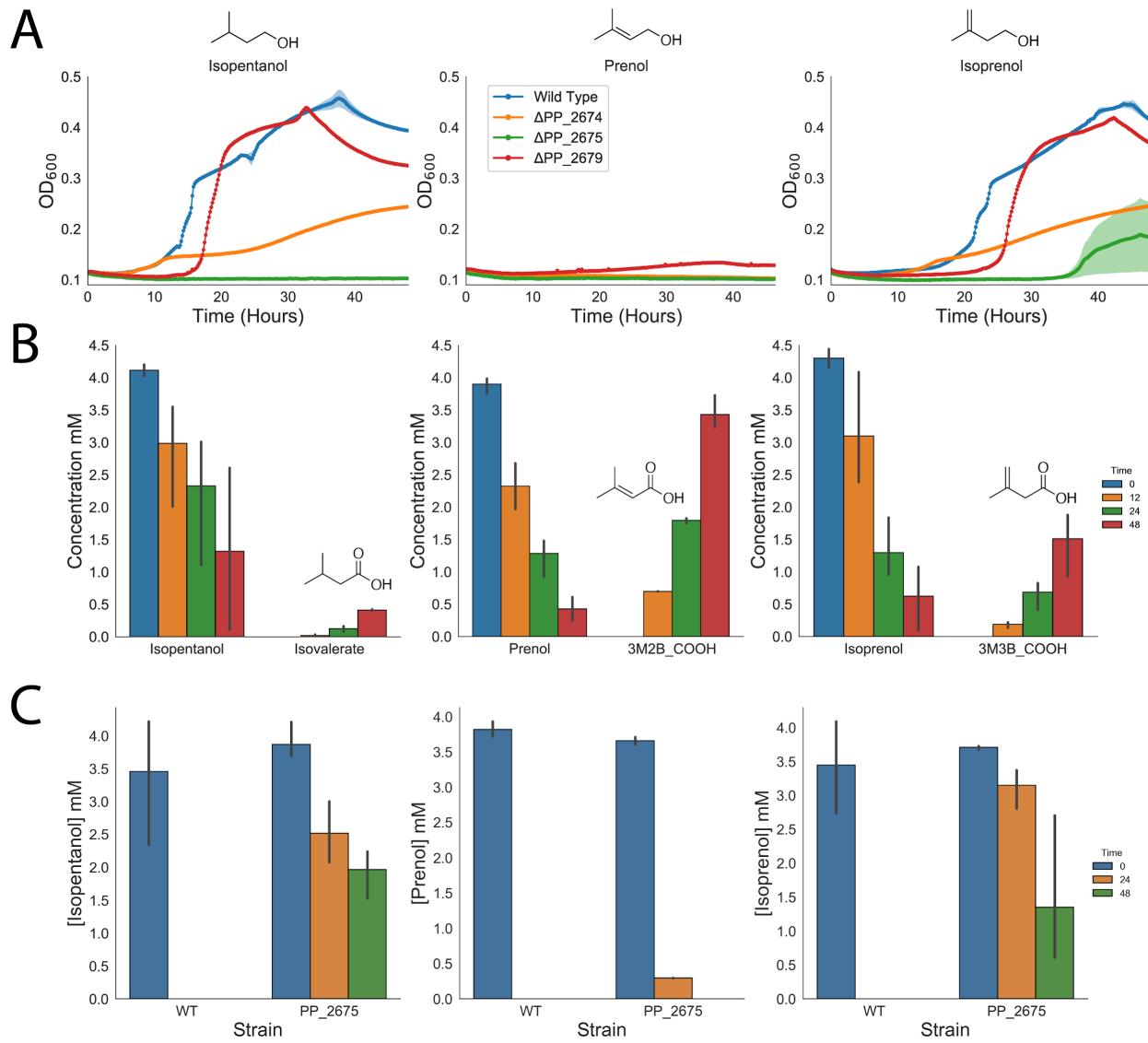
560 Branched chain alcohol metabolism

561 Due to their superior biofuel properties, branched chain alcohols have been targets for  
562 metabolic engineering as potential alternatives to ethanol and butanol (68). Our fitness data  
563 suggest that *pedE* and/or *pedH* oxidize 2-methyl-1-butanol to 2-methylbutyrate, which then

564 undergoes one round of beta-oxidation to produce acetyl-CoA and propionyl-CoA (**Figure S7**).  
565 Most of the genes involved in 2-methylbutyrate beta-oxidation are located in the operon  
566 PP\_2213-PP\_2217. With mutants having a fitness defect of -3.2, PP\_2213 appears to be the main  
567 acyl-CoA ligase acting on 2-methylbutyrate. Mutants in two predicted acyl-CoA  
568 dehydrogenases, PP\_2216 and PP\_0358, show fitness defects of -1.1 and -2.6, respectively. The  
569 enoyl-CoA hydratase PP\_2217 has a fitness defect of -5.7 and the 3-hydroxyacyl-CoA  
570 dehydrogenase PP\_2214 has a fitness defect of -5.6. Finally, the acetyl-CoA acetyltransferase  
571 appears to be PP\_2215, with mutants having a fitness defect of -4.8. We also observed fitness  
572 defects of -1.8 and -1.6 in mutants of the ABC transporters, PP\_5538 and PP\_2667, respectively.  
573 Since 2-methylbutyrate is a known intermediate in the catabolism of isoleucine, we found that  
574 the genetic data presented here closely mirror the previous biochemical characterization of this  
575 system (69, 70).

576 *P. putida* can readily grow on isopentanol and isoprenol but not prenol (**Figure 9A**). All  
577 three of these alcohols have been produced in high titers in *Escherichia coli* and other bacteria  
578 because of their potential to be suitable replacements for gasoline (71, 72). RB-TnSeq data for  
579 isopentanol and isoprenol showed severe fitness defects in genes of the leucine catabolic  
580 pathway (**Figure 10**). This is unsurprising, as isopentanol can be generated from the leucine  
581 biosynthetic pathway (73). Deletion of the PP\_4064-PP\_4067 operon, which contains the genes  
582 that code for the conversion of isovaleryl-CoA to 3-hydroxy-3-methylglutaryl-CoA, abolished  
583 growth on both isopentanol and isoprenol (**Figure S8**). Deletion of PP\_3122 (acetoacetyl CoA-  
584 transferase subunit A) also abolished growth on isopentanol, and greatly reduced growth on  
585 isoprenol (**Figure S8**). Taken together, these results validate that both of these alcohols are  
586 degraded via the leucine catabolic pathway. Transposon insertion mutants in *pedF* showed strong

587 fitness defects on both isopentanol and isoprenol, suggesting that *pedH* (PP\_2679) and *pedE*  
588 catalyze (PP\_2674) the oxidation of the alcohols. Deletion mutants in *pedH* showed only a minor  
589 delay in growth compared to wild-type when grown on either isopentanol or isoprenol, while  
590 mutants in *pedE* showed a more substantial growth defect on both alcohols (**Figure 9A**).  
591 Deletion of *pedF* (PP\_2675) prevented growth on both isopentanol and nearly abolished growth  
592 on isoprenol when provided as a sole carbon source in minimal media (**Figure 9A**). When wild-  
593 type *P. putida* was grown in minimal media with 10 mM glucose and 4 mM of either  
594 isopentanol, prenol, or isoprenol, each alcohol was shown to be readily degraded with concurrent  
595 observation of increasing levels of the resultant acid (**Figure 9B**). Though *P. putida* was unable  
596 to utilize prenol as a sole carbon source, it was still able to readily oxidize prenol to 3-methyl-2-  
597 butenoic acid, suggesting there is no CoA-ligase present in the cell able to activate this substrate  
598 and channel it towards leucine catabolism (**Figure 10**). When wild-type *P. putida* was grown in  
599 LB medium supplemented with 4 mM of each alcohol individually, all alcohols were completely  
600 degraded by 24 hours post-inoculation (**Figure 9C**). In *pedF* deletion mutants grown under the  
601 same conditions, the rate at which the alcohols were degraded was significantly slowed; however  
602 after 48 hours ~50% of isopentanol, ~75% of isoprenol, and 100% of prenol were degraded  
603 (**Figure 9C**). Uninoculated controls showed that no alcohol was lost at greater than 5% on  
604 account of evaporation (data not shown). Future efforts to produce any of these alcohols in *P.*  
605 *putida* will be heavily impacted by this degradation, and greater effort will need to be made to  
606 identify other enzymes involved in the oxidation of these alcohols or other metabolic pathways  
607 that consume them.

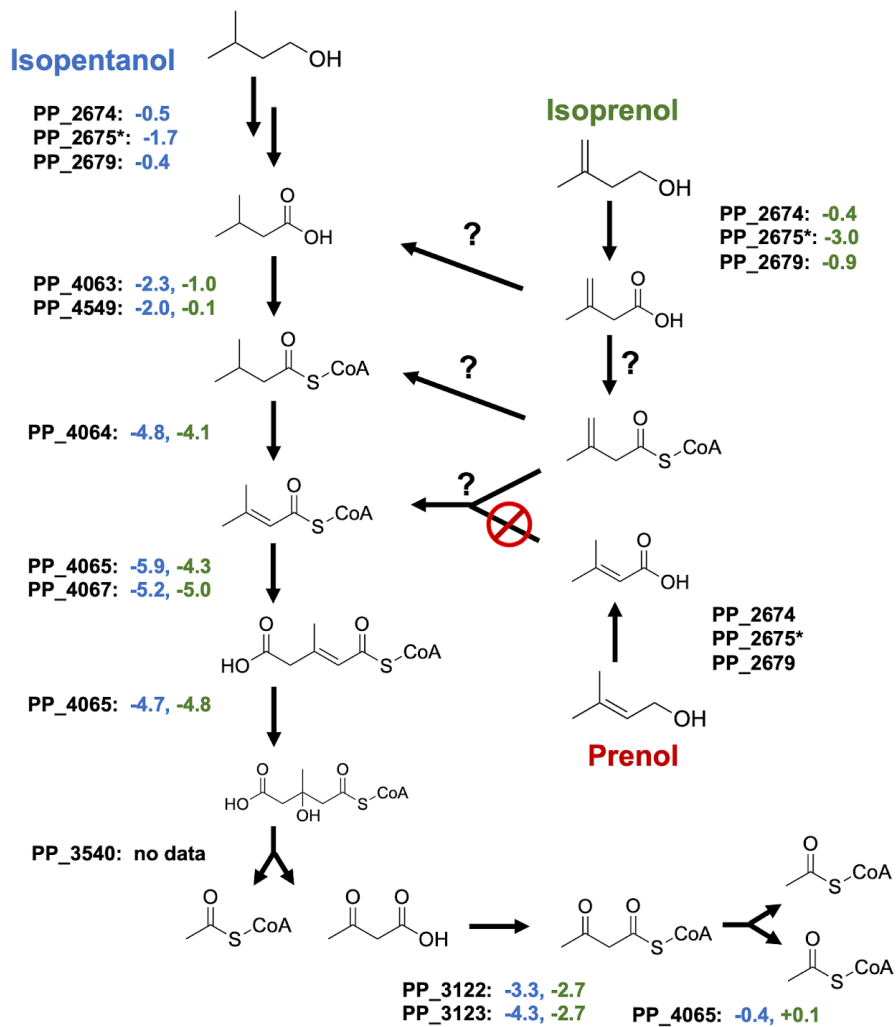


608 **Figure 9: Isopentanol, Prenol, and Isoprenol consumption by *P. putida*.** A) Growth curves of wild type (blue),  
609 and  $\Delta$ PP\_2674 (orange),  $\Delta$ PP\_2675 (green), and  $\Delta$ PP\_2679 (red) strains of *P. putida* on isopentanol (left),  
610 prenol (middle), and isoprenol (right). Structure of alcohols are shown above graphs. Shaded area represents 95%  
611 confidence intervals (CI), n=3. B) Concentrations of alcohols consumed and their corresponding carboxylic acids  
612 produced over time by wild type. Left panel shows isopentanol and isovalerate, middle panel shows prenol and 3-  
613 methyl-2-butenoic acid, and the right panel shows isoprenol and 3-methyl-3-butenoic acid. Structures of  
614 corresponding carboxylic acids derived from alcohol are shown in graphs. Error bars represent 95% CI, n=3. C)  
615 Consumption of isopentanol (left), prenol (middle), and isoprenol (right) by wild type and  $\Delta$ PP\_2675 *P. putida* over  
616 time. Error bars represent 95% CI, n=3.

618

619       One mystery that remains is how isoprenol enters into leucine catabolism. GC-MS  
620 analysis confirmed oxidation of the alcohol to 3-methyl-3-butenoic acid, but it is unclear what  
621 the next step entails. Fitness data suggests that either PP\_4063 or PP\_4549 may attach the CoA  
622 to isovalerate, but neither of these genes have strong phenotypes when mutant libraries are  
623 grown on isoprenol (**Figure 10**). That PP\_4064 (isovaleryl-CoA dehydrogenase) shows strong  
624 negative fitness values when libraries are grown on isoprenol implies that its degradation goes  
625 through an isovaleryl-CoA intermediate, however this fitness defect may be the result of polar  
626 effects that disrupt the downstream steps (**Figure 10**). One possibility is that 3-methyl-3-  
627 butenoic acid is reduced to isovalerate in the cell; however, this seems unlikely since no  
628 isovalerate was observed via GC-MS when *P. putida* was fed isoprenol and glucose. Two other  
629 possible routes could result from the activation of 3-methyl-3-butenoic acid by an undetermined  
630 CoA-ligase. If this CoA-ligase exists, it is interesting that it would have activity on 3-methyl-3-  
631 butenoic acid but not 3-methyl-2-butenoic acid, which accumulates when *P. putida* is grown in the  
632 presence of prenol. Once formed, the 3-methyl-3-butenyl-CoA could be directed into leucine  
633 catabolism via either an isomerization to 3-methylcrotonyl-CoA or a reduction to isovaleryl-  
634 CoA. Future work that leverages metabolomics to identify compounds that accumulate in leucine  
635 catabolic mutants may reveal the missing steps and help narrow the search for their enzymes.

636



637

638 **Figure 10: Putative routes of isopentanol and isoprenol catabolism in *P. putida*.** Diagram shows the proposed  
 639 pathways for the catabolism of isopentanol and isoprenol. Average fitness scores of two biological replicates for  
 640 individual genes can be found next to each gene. Fitness values for isopentanol are shown in blue, while fitness  
 641 values for isoprenol and shown in green. Potential reactions that would bring isoprenol into leucine catabolism are  
 642 marked with a question mark.

643

#### 644 Future Directions

645 The large set of global fitness data generated in this study provide an extensive and  
 646 global overview on the putative pathways of alcohol and fatty acid degradation in *P. putida*.

647 Overall, our fitness data agree with previously published biochemical data that explored enzymes  
648 in both fatty acid and alcohol metabolism. However, there are still many questions that our data  
649 leave unanswered. Further investigation will be required to untangle and elucidate which specific  
650 enzymes are biologically relevant in the beta-oxidation of short chain fatty acids. It is likely that  
651 biochemical characterization of individual enzymes will be required to determine which of the  
652 *fad* homologs catalyze these reactions. Another intriguing question is the function of PP\_0765  
653 and PP\_0766. Biochemical interrogation and mutational analysis of the DUF1302 and DUF1329  
654 family proteins are needed to determine whether these proteins indeed function as an esterase or,  
655 as previously predicted, play some other role in outer membrane biogenesis (41). Additional  
656 work is also warranted to ascertain which of the proposed 1,4-butanediol catabolic routes the  
657 wild-type organism actually uses and determine whether the beta-oxidation pathway is indeed  
658 less preferable than the pathway to succinate.

659 To our knowledge, our finding that *P. putida* can consume both isopentanol and isoprenol  
660 are the first observations of this metabolism. If metabolic engineers wish to produce these  
661 chemicals in *P. putida*, these pathways will need to be removed. Critically, researchers will need  
662 to identify other enzymes that result in the oxidation of these alcohols or other routes of  
663 degradation within *P. putida*. How *P. putida* is able to utilize isoprenol, but not prenol, as a sole  
664 carbon source is metabolically intriguing. One of our proposed pathways of isoprenol catabolism  
665 requires the existence of a CoA-ligase that shows surprising specificity towards 3-methyl-3-  
666 butenoic acid with little to no activity on 3-methyl-2-butenoic acid. More work should be done to  
667 leverage other omics-levels techniques to try to identify this hypothetical enzyme and  
668 biochemically verify its activity. Finally, this data set as a whole will likely strengthen the  
669 assumptions made by genome-scale metabolic models. Previous models of *P. putida* metabolism

670 have incorporated RB-TnSeq data to improve their predictions (17). This work nearly doubles  
671 the number of available RB-TnSeq datasets in *P. putida* that are publicly available and will likely  
672 contribute greatly to further model refinement. Ultimately, large strides in our understanding of  
673 *P. putida* metabolism leveraging functional genomic approaches will provide the foundation for  
674 improved metabolic engineering efforts in the future.

675

## 676 **Methods**

### 677 Media, chemicals, and culture conditions

678 General *E. coli* cultures were grown in lysogeny broth (LB) Miller medium (BD  
679 Biosciences, USA) at 37 °C while *P. putida* was grown at 30 °C. When indicated, *P. putida* and  
680 *E. coli* were grown on modified MOPS minimal medium, which is comprised of 32.5 µM CaCl<sub>2</sub>,  
681 0.29 mM K<sub>2</sub>SO<sub>4</sub>, 1.32 mM K<sub>2</sub>HPO<sub>4</sub>, 8 µM FeCl<sub>2</sub>, 40 mM MOPS, 4 mM tricine, 0.01 mM  
682 FeSO<sub>4</sub>, 9.52 mM NH<sub>4</sub>Cl, 0.52 mM MgCl<sub>2</sub>, 50 mM NaCl, 0.03 µM (NH<sub>4</sub>)<sub>6</sub>Mo<sub>7</sub>O<sub>24</sub>, 4 µM H<sub>3</sub>BO<sub>3</sub>,  
683 0.3 µM CoCl<sub>2</sub>, 0.1 µM CuSO<sub>4</sub>, 0.8 µM MnCl<sub>2</sub>, and 0.1 µM ZnSO<sub>4</sub> (74). Cultures were  
684 supplemented with kanamycin (50 mg/L, Sigma Aldrich, USA), gentamicin (30 mg/L, Fisher  
685 Scientific, USA), or carbenicillin (100mg/L, Sigma Aldrich, USA), when indicated. All other  
686 compounds were purchased through Sigma Aldrich (Sigma Aldrich, USA). 3-methyl-3-butenoic  
687 acid was not available commercially and required synthesis which is described below.

### 688 Strains and plasmids

689 All bacterial strains and plasmids used in this work are listed in Table 1. All strains and  
690 plasmids created in this work are available through the public instance of the JBEI registry.  
691 ([public-registry.jbei.org/folders/456](https://public-registry.jbei.org/folders/456)). All plasmids were designed using Device Editor and  
692 Vector Editor software, while all primers used for the construction of plasmids were designed

693 using j5 software (75–77). Plasmids were assembled via Gibson Assembly using standard  
694 protocols (78), or Golden Gate Assembly using standard protocols (79). Plasmids were routinely  
695 isolated using the Qiaprep Spin Miniprep kit (Qiagen, USA), and all primers were purchased  
696 from Integrated DNA Technologies (IDT, Coralville, IA). Construction of *P. putida* deletion  
697 mutants was performed as described previously (18).

698 **Table 1: Strains and plasmids used in this study.**

Strain	Description	Reference
<i>E. coli</i> XL1 Blue		Agilent
<i>P. putida</i> KT2440	Wild-Type	ATCC 47054
<i>P. putida</i> ΔPP_2674	Strain with complete internal in-frame deletion of PP_2674	This study
<i>P. putida</i> ΔPP_2675	Strain with complete internal in-frame deletion of PP_2675	This study
<i>P. putida</i> ΔPP_2679	Strain with complete internal in-frame deletion of PP_2679	This study
<i>P. putida</i> ΔPP_3839	Strain with complete internal in-frame deletion of PP_3839	This study
<i>P. putida</i> ΔPP_2675 ΔPP_3839	A double knockout of PP_2675 and PP_3839	This study
<i>P. putida</i> ΔPP_4064-PP_4067	Strain with complete internal in-frame deletion of the PP_4064-4067 operon	This study

<i>P. putida</i> ΔPP_3122	Strain with complete internal in-frame deletion of PP_3122	This study
<b>Plasmids</b>		
pMQ30	Suicide vector for allelic replace Gm <sup>r</sup> , SacB	(80)
pMQ30 ΔPP_2674	pMQ30 derivative harboring 1kb flanking regions of PP_2674	This study
pMQ30 ΔPP_2675	pMQ30 derivative harboring 1kb flanking regions of PP_2675	This study
pMQ30 ΔPP_2679	pMQ30 derivative harboring 1kb flanking regions of PP_2679	This study
pMQ30 ΔPP_3839	pMQ30 derivative harboring 1kb flanking regions of PP_3839	This study
pMQ30 ΔPP_4064-PP_4067	pMQ30 derivative harboring 1kb flanking regions of PP_4064 and PP_4067	This study
pMQ30 ΔPP_3122	pMQ30 derivative harboring 1kb flanking regions of PP_3122	This study

699  
700

701 Plate-based growth assays

702 Growth studies of bacterial strains were conducted using microplate reader kinetic assays  
703 as described previously (81). Overnight cultures were inoculated into 10 mL of LB medium from  
704 single colonies, and grown at 30 °C. These cultures were then washed twice with MOPS minimal

705 media without any added carbon and diluted 1:100 into 500  $\mu$ L of MOPS medium with 10 mM  
706 of a carbon source in 48-well plates (Falcon, 353072). Plates were sealed with a gas-permeable  
707 microplate adhesive film (VWR, USA), and then optical density and fluorescence were  
708 monitored for 48 hours in an Biotek Synergy 4 plate reader (BioTek, USA) at 30 °C with fast  
709 continuous shaking. Optical density was measured at 600 nm.

710 RB-TnSeq

711 RB-TnSeq experiments utilized *P. putida* library JBEI-1 which has been described  
712 previously with slight modification(18). Libraries of JBEI-1 were thawed on ice, diluted into 25  
713 mL of LB medium with kanamycin and then grown to an OD<sub>600</sub> of 0.5 at 30 °C at which point  
714 three 1-mL aliquots were removed, pelleted, and stored at -80 °C. Libraries were then washed  
715 once in MOPS minimal medium with no carbon source, and then diluted 1:50 in MOPS minimal  
716 medium with 10 mM of each carbon source tested. Cells were grown in 10 mL of medium in test  
717 tubes at 30 °C shaking at 200 rpm. One 500- $\mu$ L aliquot was pelleted, and stored at -80 °C until  
718 BarSeq analysis, which was performed as previously described (19, 40). The fitness of a strain is  
719 defined here as the normalized log<sub>2</sub> ratio of barcode reads in the experimental sample to barcode  
720 reads in the time zero sample. The fitness of a gene is defined here as the weighted average of  
721 the strain fitness for insertions in the central 10% to 90% of the gene. The gene fitness values are  
722 normalized such that the typical gene has a fitness of zero. The primary statistic *t* value  
723 represents the form of fitness divided by the estimated variance across different mutants of the  
724 same gene. Statistic *t* values of  $>|4|$  were considered significant. A more detailed explanation of  
725 calculating fitness scores can be found in Wetmore et al. (40). All experiments described here  
726 passed testing using the quality metrics described previously unless noted otherwise (40). All

727 experiments were conducted in biological duplicate, and all fitness data are publically available  
728 at <http://fit.genomics.lbl.gov>.

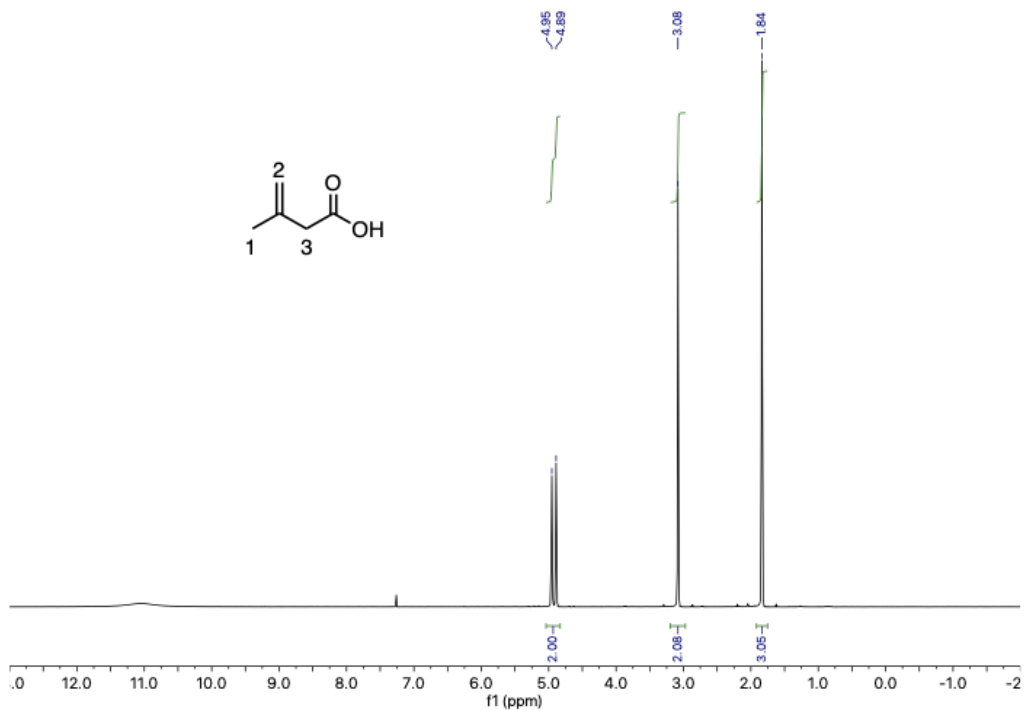
729 GC-MS and GC-FID Analysis of Branched Alcohol Consumption

730 To examine the oxidation of isopentanol, prenol, and isoprenol to their corresponding  
731 acids 10mL of MOPS minimal medium supplemented with 10 mM glucose and 4mM of one of  
732 each alcohol added were inoculated with a 1:100 dilution of overnight *P. putida* culture and  
733 incubated at 30 °C with 200 rpm shaking. At 0, 12, 24, and 48-hours post-inoculation 200 µL of  
734 media were sampled and stored at - 80 °C. Alcohols and fatty acids were extracted by acidifying  
735 media with 10 µL of 10N HCl, followed by addition of an 200 µL of ethyl-acetate. To detect  
736 alcohols and their corresponding carboxylic acids via GC-MS an Agilent 6890 system equipped  
737 with a DB-5ms column (30- m×0.25 mm×0.25 µm) and an Agilent 5973 MS were used. Helium  
738 (constant flow 1 mL/min) was used as the carrier gas. The temperature of the injector was 250 °C  
739 and the following temperature program was applied: 40 °C for 2 min, increase of 10 °C/min to  
740 100 °C then increase of 35 °C/min to 300 °C , temperature was then held at 300 °C for 1 min.  
741 Authentic standards were used to quantify analytes. Determination of isopentanol, prenol, and  
742 isoprenol consumption was conducted in 10mL LB medium with 4mM of either alcohol added.  
743 Cultures were inoculated with a 1:100 dilution of overnight *P. putida* culture and incubated at  
744 30 °C with 200 rpm shaking. At 0, 24, and 48 hours post-inoculation 200 µL of media were  
745 sampled and stored at - 80 °C. The remaining concentration of each alcohol was determined by  
746 GC-FID as previously described (82).

747 Synthesis of 3-Methyl-3-Butenoic Acid

748 To a 25-mL round bottom flask was added chromium(VI) oxide (0.69 g, 6.9 mmol) and distilled  
749 water (1 mL). The reaction mixture was then cooled to 0 °C before concentrated sulfuric acid (0.6

750 mL, 10.5 mmol) was added dropwise, thus forming Jones reagent.  
751 The solution of Jones reagent was then diluted to a total volume of 5 mL with distilled water. To a stirred solution of 3-methyl-  
752 3-buten-1-ol (0.59 g, 6.9 mmol) in acetone (7 ml) was added dropwise the Jones reagent at 0 °C.  
753 After being stirred for 8 h at room temperature, the mixture was quenched with ethanol. The  
754 mixture was then diluted with water, and acetone was evaporated *in vacuo*. The residue was  
755 extracted with DCM, and organic layers were combined and washed three times with saturated *aq.*  
756 NaHCO<sub>3</sub> solution. The aqueous phase was acidified with a 2 M *aq.* HCl solution to pH 2-3, which  
757 was then extracted again with DCM. The extract was successively washed with water and brine,  
758 dried over MgSO<sub>4</sub>, and concentrated *in vacuo*. The residue was distilled (90 °C, 100 mTorr) to  
759 yield 3-methyl-3-butenoic acid as a clear oil. <sup>1</sup>H NMR (300 MHz, Chloroform-*d*) δ 4.92 (d, *J* =  
760 19.1 Hz, 2H), 3.08 (s, 2H), 1.84 (s, 3H) (**Figure 10**).



761

762 **Figure 11: NMR validation of 3-methyl-3-butenoic acid.**

763

764 Bioinformatic Analyses

765 PaperBLAST was routinely used to search for literature on proteins of interest and related  
766 homologs (61). All statistical analyses were carried out using either the Python Scipy or Numpy  
767 libraries (83, 84). For the phylogenetic reconstructions, the best amino acid substitution model  
768 was selected using ModelFinder as implemented on IQ-tree (85) phylogenetic trees were  
769 constructed using IQ-tree, nodes were supported with 10,000 bootstrap replicates. The final tree  
770 figures were edited using FigTree v1.4.3 (<http://tree.bio.ed.ac.uk/software/figtree/>). Orthologous  
771 syntenic regions were identified with CORASON-BGC (86) and manually colored and  
772 annotated.

773 **Acknowledgements**

774 We would like to thank Morgan Price for assistance in analyzing RB-TnSeq data. The  
775 laboratory of LMB is partially funded by the Deutsche Forschungsgemeinschaft (DFG, German  
776 Research Foundation) under Germany's Excellence Strategy within the Cluster of Excellence  
777 FSC 2186 'The Fuel Science Center'. This work was part of the DOE Joint BioEnergy Institute  
778 (<https://www.jbei.org>) supported by the U. S. Department of Energy, Office of Science, Office of  
779 Biological and Environmental Research, supported by the U.S. Department of Energy, Energy  
780 Efficiency and Renewable Energy, Bioenergy Technologies Office, through contract DE-AC02-  
781 05CH11231 between Lawrence Berkeley National Laboratory and the U.S. Department of  
782 Energy. The views and opinions of the authors expressed herein do not necessarily state or  
783 reflect those of the United States Government or any agency thereof. Neither the United States  
784 Government nor any agency thereof, nor any of their employees, makes any warranty, expressed  
785 or implied, or assumes any legal liability or responsibility for the accuracy, completeness, or  
786 usefulness of any information, apparatus, product, or process disclosed, or represents that its use

787 would not infringe privately owned rights. The United States Government retains and the  
788 publisher, by accepting the article for publication, acknowledges that the United States  
789 Government retains a nonexclusive, paid-up, irrevocable, worldwide license to publish or  
790 reproduce the published form of this manuscript, or allow others to do so, for United States  
791 Government purposes. The Department of Energy will provide public access to these results of  
792 federally sponsored research in accordance with the DOE Public Access Plan  
793 (<http://energy.gov/downloads/doe-public-access-plan>).  
794

## 795 **Contributions**

796 Conceptualization, M.G.T., M.R.I., A.N.P.; Methodology, M.G.T., M.R.I., A.N.P., J.M.B.,  
797 P.C.M., A.M.D.; Investigation, M.G.T., M.R.I., A.N.P., M.S., W.A.S., C.B.E., P.C.M., J.M.B.,  
798 Y.L., R.W.H., C.A.A, R.N.K, P.L.; Writing – Original Draft, M.G.T., M.R.I., A.N.P.; Writing –  
799 Review and Editing, All authors.; Resources and supervision, L.M.B., A.M., A.M.D., P.M.S.,  
800 J.D.K.

801 M.G.T., M.R.I., and A.N.P. contributed equally to this work. Author order was determined by  
802 the outcome of a MarioKart 64 tournament.

## 803 **Competing Interests**

804 J.D.K. has financial interests in Amyris, Lygos, Demetrix, Napigen, Maple Bio, and Apertor  
805 Labs. C.B.E has a financial interest in Perlumi Chemicals.

806     **Bibliography**

807     1.     **Park M, Chen Y, Thompson M, Benites VT, Fong B, Petzold CJ, Baidoo EEK, Gladden JM, Adams PD, Keasling JD, Simmons BA, Singer SW. 2020. Response of *Pseudomonas putida* to Complex, Aromatic-Rich Fractions from Biomass.**

808     **ChemSusChem 13:1–14.**

809

810

811     2.     **Belda E, van Heck RGA, José Lopez-Sanchez M, Cruveiller S, Barbe V, Fraser C, Klenk H-P, Petersen J, Morgat A, Nikel PI, Vallenet D, Rouy Z, Sekowska A, Martins Dos Santos VAP, de Lorenzo V, Danchin A, Médigue C. 2016. The revisited genome of *Pseudomonas putida* KT2440 enlightens its value as a robust metabolic chassis.**

812     **Environ Microbiol 18:3403–3424.**

813

814

815

816     3.     **Tiso T, Narancic T, Wei R, Pollet E, Beagan N, Schröder K, Honak A, Jiang M, Kenny ST, Wierckx N, Perrin R, Avérous L, Zimmermann W, O'Connor K, Blank LM. 2020. Bio-upcycling of polyethylene terephthalate.**

817     **BioRxiv.**

818

819     4.     **Aparicio T, de Lorenzo V, Martínez-García E. 2019. CRISPR/Cas9-enhanced ssDNA recombineering for *Pseudomonas putida*.**

820     **Microb Biotechnol 12:1076–1089.**

821

822

823     5.     **Aparicio T, de Lorenzo V, Martínez-García E. 2018. CRISPR/Cas9-Based Counterselection Boosts Recombineering Efficiency in *Pseudomonas putida*.**

824     **Biotechnol J 13:e1700161.**

825

826

827     6.     **Cook TB, Rand JM, Nurani W, Courtney DK, Liu SA, Pfleger BF. 2018. Genetic tools for reliable gene expression and recombineering in *Pseudomonas putida*.**

828     **J Ind Microbiol Biotechnol 45:517–527.**

829

830     7.     **Banerjee D, Eng TT, Lau AK, Wang B, Sasaki Y, Herbert RA, Chen Y, Liu Y, Prahl**

828                   **J-P, Singan VR, Tanjore D, Petzold CJ, Keasling JD, Mukhopadhyay A. 2020.**  
829                   **Genome-scale metabolic rewiring to achieve predictable titers rates and yield of a**  
830                   **non-native product at scale. BioRxiv.**

831           **8. Blank LM, Ionidis G, Ebert BE, Bühler B, Schmid A. 2008. Metabolic response of**  
832                   **Pseudomonas putida during redox biocatalysis in the presence of a second octanol**  
833                   **phase. FEBS J 275:5173–5190.**

834           **9. Ebert BE, Kurth F, Grund M, Blank LM, Schmid A. 2011. Response of**  
835                   **Pseudomonas putida KT2440 to increased NADH and ATP demand. Appl Environ**  
836                   **Microbiol 77:6597–6605.**

837           **10. Thompson MG, Valencia LE, Blake-Hedges JM, Cruz-Morales P, Velasquez AE,**  
838                   **Pearson AN, Sermenio LN, Sharpless WA, Benites VT, Chen Y, Baidoo EEK, Petzold**  
839                   **CJ, Deutschbauer AM, Keasling JD. 2019. Omics-driven identification and**  
840                   **elimination of valerolactam catabolism in Pseudomonas putida KT2440 for increased**  
841                   **product titer. Metab Eng Commun 9:e00098.**

842           **11. Incha MR, Thompson MG, Blake-Hedges JM, Liu Y, Pearson AN, Schmidt M, Gin**  
843                   **JW, Petzold CJ, Deutschbauer AM, Keasling JD. 2020. Leveraging host metabolism**  
844                   **for bisdemethoxycurcumin production in Pseudomonas putida. Metab Eng Commun**  
845                   **10:e00119.**

846           **12. Zhang M, Gao C, Guo X, Guo S, Kang Z, Xiao D, Yan J, Tao F, Zhang W, Dong W,**  
847                   **Liu P, Yang C, Ma C, Xu P. 2018. Increased glutarate production by blocking the**  
848                   **glutaryl-CoA dehydrogenation pathway and a catabolic pathway involving L-2-**  
849                   **hydroxyglutarate. Nat Commun 9:2114.**

850 13. Dong J, Chen Y, Benites VT, Baidoo EEK, Petzold CJ, Beller HR, Eudes A, Scheller  
851 HV, Adams PD, Mukhopadhyay A, Simmons BA, Singer SW. 2019. Methyl ketone  
852 production by *Pseudomonas putida* is enhanced by plant-derived amino acids.  
853 *Biotechnol Bioeng* 116:1909–1922.

854 14. Tiso T, Zauter R, Tulke H, Leuchtle B, Li W-J, Behrens B, Wittgens A, Rosenau F,  
855 Hayen H, Blank LM. 2017. Designer rhamnolipids by reduction of congener  
856 diversity: production and characterization. *Microb Cell Fact* 16:225.

857 15. Kohlstedt M, Starck S, Barton N, Stolzenberger J, Selzer M, Mehlmann K,  
858 Schneider R, Pleissner D, Rinkel J, Dickschat JS, Venus J, B J H van Duuren J,  
859 Wittmann C. 2018. From lignin to nylon: Cascaded chemical and biochemical  
860 conversion using metabolically engineered *Pseudomonas putida*. *Metab Eng* 47:279–  
861 293.

862 16. Loeschke A, Thies S. 2020. Engineering of natural product biosynthesis in  
863 *Pseudomonas putida*. *Curr Opin Biotechnol* 65:213–224.

864 17. Nogales J, Mueller J, Gudmundsson S, Canalejo FJ, Duque E, Monk J, Feist AM,  
865 Ramos JL, Niu W, Palsson BO. 2020. High-quality genome-scale metabolic  
866 modelling of *Pseudomonas putida* highlights its broad metabolic capabilities.  
867 *Environ Microbiol* 22:255–269.

868 18. Thompson MG, Blake-Hedges JM, Cruz-Morales P, Barajas JF, Curran SC, Eiben  
869 CB, Harris NC, Benites VT, Gin JW, Sharpless WA, Twigg FF, Skyrud W, Krishna  
870 RN, Pereira JH, Baidoo EEK, Petzold CJ, Adams PD, Arkin AP, Deutschbauer AM,  
871 Keasling JD. 2019. Massively Parallel Fitness Profiling Reveals Multiple Novel

872       **Enzymes in *Pseudomonas putida* Lysine Metabolism. MBio 10.**

873   **19. Rand JM, Pisithkul T, Clark RL, Thiede JM, Mehrer CR, Agnew DE, Campbell CE,**  
874       **Markley AL, Price MN, Ray J, Wetmore KM, Suh Y, Arkin AP, Deutschbauer AM,**  
875       **Amador-Noguez D, Pfleger BF. 2017. A metabolic pathway for catabolizing levulinic**  
876       **acid in bacteria. Nat Microbiol 2:1624–1634.**

877   **20. Price MN, Ray J, Iavarone AT, Carlson HK, Ryan EM, Malmstrom RR, Arkin AP,**  
878       **Deutschbauer AM. 2019. Oxidative pathways of deoxyribose and deoxyribonate**  
879       **catabolism. mSystems 4.**

880   **21. Zhu Z, Hu Y, Teixeira PG, Pereira R, Chen Y, Siewers V, Nielsen J. 2020.**  
881       **Multidimensional engineering of *Saccharomyces cerevisiae* for efficient synthesis of**  
882       **medium-chain fatty acids. Nat Catal 3:64–74.**

883   **22. Luo X, Reiter MA, d'Espaux L, Wong J, Denby CM, Lechner A, Zhang Y,**  
884       **Grzybowski AT, Harth S, Lin W, Lee H, Yu C, Shin J, Deng K, Benites VT, Wang**  
885       **G, Baidoo EEK, Chen Y, Dev I, Petzold CJ, Keasling JD. 2019. Complete**  
886       **biosynthesis of cannabinoids and their unnatural analogues in yeast. Nature**  
887       **567:123–126.**

888   **23. Mehrer CR, Incha MR, Politz MC, Pfleger BF. 2018. Anaerobic production of**  
889       **medium-chain fatty alcohols via a  $\beta$ -reduction pathway. Metab Eng 48:63–71.**

890   **24. Karp PD, Billington R, Caspi R, Fulcher CA, Latendresse M, Kothari A, Keseler IM,**  
891       **Krummenacker M, Midford PE, Ong Q, Ong WK, Paley SM, Subhraveti P. 2019.**  
892       **The BioCyc collection of microbial genomes and metabolic pathways. Brief**  
893       **Bioinformatics 20:1085–1093.**

894 25. Wehrmann M, Billard P, Martin-Meriadec A, Zegeye A, Klebensberger J. 2017.  
895       **Functional Role of Lanthanides in Enzymatic Activity and Transcriptional**  
896       **Regulation of Pyrroloquinoline Quinone-Dependent Alcohol Dehydrogenases in**  
897       **Pseudomonas putida KT2440.** *MBio* 8.

898 26. Wehrmann M, Toussaint M, Pfannstiel J, Billard P, Klebensberger J. 2020. The  
899       **Cellular Response to Lanthanum Is Substrate Specific and Reveals a Novel Route for**  
900       **Glycerol Metabolism in Pseudomonas putida KT2440.** *MBio* 11.

901 27. Nikel PI, de Lorenzo V. 2014. Robustness of *Pseudomonas putida* KT2440 as a host  
902       for ethanol biosynthesis. *N Biotechnol* 31:562–571.

903 28. Cuenca M del S, Roca A, Molina-Santiago C, Duque E, Armengaud J, Gómez-  
904       Garcia MR, Ramos JL. 2016. Understanding butanol tolerance and assimilation in  
905       *Pseudomonas putida* BIRD-1: an integrated omics approach. *Microb Biotechnol*  
906       9:100–115.

907 29. Simon O, Klebensberger J, Mükschel B, Klaiber I, Graf N, Altenbuchner J, Huber  
908       A, Hauer B, Pfannstiel J. 2015. Analysis of the molecular response of *Pseudomonas*  
909       *putida* KT2440 to the next-generation biofuel n-butanol. *J Proteomics* 122:11–25.

910 30. Li W-J, Narancic T, Kenny ST, Niehoff P-J, O'Connor K, Blank LM, Wierckx N.  
911       2020. Unraveling 1,4-Butanediol Metabolism in *Pseudomonas putida* KT2440. *Front*  
912       *Microbiol* 11:382.

913 31. Basler G, Thompson M, Tullman-Ercek D, Keasling J. 2018. A *Pseudomonas putida*  
914       efflux pump acts on short-chain alcohols. *Biotechnol Biofuels* 11:136.

915 32. Nikel PI, Chavarría M, Danchin A, de Lorenzo V. 2016. From dirt to industrial

916 applications: **Pseudomonas putida** as a Synthetic Biology chassis for hosting harsh  
917 biochemical reactions. **Curr Opin Chem Biol** 34:20–29.

918 33. **Burlage RS, Hooper SW, Sayler GS.** 1989. The TOL (pWW0) catabolic plasmid.  
919 **Appl Environ Microbiol** 55:1323–1328.

920 34. **Nozzi NE, Desai SH, Case AE, Atsumi S.** 2014. Metabolic engineering for higher  
921 alcohol production. **Metab Eng** 25:174–182.

922 35. **Yan Q, Pfleger BF.** 2020. Revisiting metabolic engineering strategies for microbial  
923 synthesis of oleochemicals. **Metab Eng** 58:35–46.

924 36. **Pfleger BF, Gossing M, Nielsen J.** 2015. Metabolic engineering strategies for  
925 microbial synthesis of oleochemicals. **Metab Eng** 29:1–11.

926 37. **Kukurugya MA, Mendonca CM, Solhtalab M, Wilkes RA, Thannhauser TW,**  
927 **Aristilde L.** 2019. Multi-omics analysis unravels a segregated metabolic flux network  
928 that tunes co-utilization of sugar and aromatic carbons in **Pseudomonas putida**. **J**  
929 **Biol Chem** 294:8464–8479.

930 38. **Nikel PI, Fuhrer T, Chavarria M, Sanchez-Pascuala A, Sauer U, de Lorenzo V.** 2020.  
931 **Redox stress reshapes carbon fluxes of Pseudomonas putida for cytosolic glucose**  
932 **oxidation and NADPH generation.** **BioRxiv**.

933 39. **Nikel PI, Chavarría M, Fuhrer T, Sauer U, de Lorenzo V.** 2015. *Pseudomonas putida*  
934 **KT2440 Strain Metabolizes Glucose through a Cycle Formed by Enzymes of the**  
935 **Entner-Doudoroff, Embden-Meyerhof-Parnas, and Pentose Phosphate Pathways.** **J**  
936 **Biol Chem** 290:25920–25932.

937 40. **Wetmore KM, Price MN, Waters RJ, Lamson JS, He J, Hoover CA, Blow MJ,**

938                   **Bristow J, Butland G, Arkin AP, Deutschbauer A. 2015. Rapid quantification of**  
939                   **mutant fitness in diverse bacteria by sequencing randomly bar-coded transposons.**

940                   **MBio 6:e00306-15.**

941           **41. Price MN, Wetmore KM, Waters RJ, Callaghan M, Ray J, Liu H, Kuehl JV, Melnyk**  
942           **RA, Lamson JS, Suh Y, Carlson HK, Esquivel Z, Sadeeshkumar H, Chakraborty R,**  
943           **Zane GM, Rubin BE, Wall JD, Visel A, Bristow J, Blow MJ, Deutschbauer AM.**

944           **2018. Mutant phenotypes for thousands of bacterial genes of unknown function.**

945           **Nature 557:503–509.**

946           **42. Guzik MW, Narancic T, Ilic-Tomic T, Vojnovic S, Kenny ST, Casey WT, Duane GF,**  
947           **Casey E, Woods T, Babu RP, Nikodinovic-Runic J, O'Connor KE. 2014.**

948           **Identification and characterization of an acyl-CoA dehydrogenase from**  
949           **Pseudomonas putida KT2440 that shows preference towards medium to long chain**  
950           **length fatty acids. Microbiology (Reading, Engl) 160:1760–1771.**

951           **43. Hume AR, Nikodinovic-Runic J, O'Connor KE. 2009. FadD from Pseudomonas**  
952           **putida CA-3 is a true long-chain fatty acyl coenzyme A synthetase that activates**  
953           **phenylalkanoic and alkanoic acids. J Bacteriol 191:7554–7565.**

954           **44. McMahon B, Mayhew SG. 2007. Identification and properties of an inducible**  
955           **phenylacyl-CoA dehydrogenase in Pseudomonas putida KT2440. FEMS Microbiol**  
956           **Lett 273:50–57.**

957           **45. Leščić Ašler I, Ivić N, Kovačić F, Schell S, Knorr J, Krauss U, Wilhelm S, Kojić-**  
958           **Prodić B, Jaeger K-E. 2010. Probing enzyme promiscuity of SGNH hydrolases.**

959           **Chembiochem 11:2158–2167.**

960 46. McMahon B, Gallagher ME, Mayhew SG. 2005. The protein coded by the PP2216  
961 gene of *Pseudomonas putida* KT2440 is an acyl-CoA dehydrogenase that oxidises  
962 only short-chain aliphatic substrates. *FEMS Microbiol Lett* 250:121–127.

963 47. del Peso-Santos T, Bartolomé-Martín D, Fernández C, Alonso S, García JL, Díaz E,  
964 Shingler V, Perera J. 2006. Coregulation by phenylacetyl-coenzyme A-responsive  
965 PaaX integrates control of the upper and lower pathways for catabolism of styrene  
966 by *Pseudomonas* sp. strain Y2. *J Bacteriol* 188:4812–4821.

967 48. Ferrández A, García JL, Díaz E. 2000. Transcriptional regulation of the divergent  
968 paa catabolic operons for phenylacetic acid degradation in *Escherichia coli*. *J Biol  
969 Chem* 275:12214–12222.

970 49. Görisch H. 2003. The ethanol oxidation system and its regulation in *Pseudomonas*  
971 *aeruginosa*. *Biochimica et Biophysica Acta (BBA) - Proteins and Proteomics*  
972 1647:98–102.

973 50. Hempel N, Görisch H, Mern DS. 2013. Gene ercA, encoding a putative iron-  
974 containing alcohol dehydrogenase, is involved in regulation of ethanol utilization in  
975 *Pseudomonas aeruginosa*. *J Bacteriol* 195:3925–3932.

976 51. Wehrmann M, Berthelot C, Billard P, Klebensberger J. 2018. The PedS2/PedR2  
977 Two-Component System Is Crucial for the Rare Earth Element Switch in  
978 *Pseudomonas putida* KT2440. *mSphere* 3.

979 52. Arias S, Olivera ER, Arcos M, Naharro G, Luengo JM. 2008. Genetic analyses and  
980 molecular characterization of the pathways involved in the conversion of 2-  
981 phenylethylamine and 2-phenylethanol into phenylacetic acid in *Pseudomonas*

982 putida U. Environ Microbiol 10:413–432.

983 53. Fernández M, Conde S, de la Torre J, Molina-Santiago C, Ramos J-L, Duque E.

984 2012. Mechanisms of resistance to chloramphenicol in *Pseudomonas putida* KT2440.

985 Antimicrob Agents Chemother 56:1001–1009.

986 54. Gliese N, Khodaverdi V, Görisch H. 2010. The PQQ biosynthetic operons and their

987 transcriptional regulation in *Pseudomonas aeruginosa*. Arch Microbiol 192:1–14.

988 55. García-Hidalgo J, Brink DP, Ravi K, Paul CJ, Lidén G, Gorwa-Grauslund MF.

989 2020. Vanillin Production in *Pseudomonas*: Whole-Genome Sequencing of

990 *Pseudomonas* sp. Strain 9.1 and Reannotation of *Pseudomonas putida* CalA as a

991 Vanillin Reductase. Appl Environ Microbiol 86.

992 56. Heeb S, Haas D. 2001. Regulatory roles of the GacS/GacA two-component system in

993 plant-associated and other gram-negative bacteria. Mol Plant Microbe Interact

994 14:1351–1363.

995 57. Venturi V. 2003. Control of *rpoS* transcription in *Escherichia coli* and *Pseudomonas*:

996 why so different? Mol Microbiol 49:1–9.

997 58. Bentley GJ, Narayanan N, Jha RK, Salvachúa D, Elmore JR, Peabody GL, Black

998 BA, Ramirez K, De Capite A, Michener WE, Werner AZ, Klingeman DM, Schindel

999 HS, Nelson R, Foust L, Guss AM, Dale T, Johnson CW, Beckham GT. 2020.

1000 Engineering glucose metabolism for enhanced muconic acid production in

1001 *Pseudomonas putida* KT2440. Metab Eng 59:64–75.

1002 59. Ryan WJ, O’Leary ND, O’Mahony M, Dobson ADW. 2013. GacS-dependent

1003 regulation of polyhydroxyalkanoate synthesis in *Pseudomonas putida* CA-3. Appl

1004                   **Environ Microbiol 79:1795–1802.**

1005   **60.** **Jacob K, Rasmussen A, Tyler P, Servos MM, Sylla M, Prado C, Daniele E, Sharp JS,**  
1006                   **Purdy AE. 2017. Regulation of acetyl-CoA synthetase transcription by the CrbS/R**  
1007                   **two-component system is conserved in genetically diverse environmental pathogens.**  
1008                   **PLoS ONE 12:e0177825.**

1009   **61.** **Price MN, Arkin AP. 2017. PaperBLAST: Text Mining Papers for Information**  
1010                   **about Homologs. mSystems 2.**

1011   **62.** **Monteagudo-Cascales E, García-Mauriño SM, Santero E, Canosa I. 2019.**  
1012                   **Unraveling the role of the CbrA histidine kinase in the signal transduction of the**  
1013                   **CbrAB two-component system in Pseudomonas putida. Sci Rep 9:9110.**

1014   **63.** **Valentini M, García-Mauriño SM, Pérez-Martínez I, Santero E, Canosa I, Lapouge**  
1015                   **K. 2014. Hierarchical management of carbon sources is regulated similarly by the**  
1016                   **CbrA/B systems in Pseudomonas aeruginosa and Pseudomonas putida. Microbiology**  
1017                   **(Reading, Engl) 160:2243–2252.**

1018   **64.** **Werle P, Morawietz M, Lundmark S, Sörensen K, Karvinen E, Lehtonen J. 2000.**  
1019                   **Alcohols, Polyhydric, p. . In Wiley-VCH Verlag GmbH & Co. KGaA (ed.),**  
1020                   **Ullmann's encyclopedia of industrial chemistry. Wiley-VCH Verlag GmbH & Co.**  
1021                   **KGaA, Weinheim, Germany.**

1022   **65.** **Wang Y, Lv M, Zhang Y, Xiao X, Jiang T, Zhang W, Hu C, Gao C, Ma C, Xu P.**  
1023                   **2014. Reconstruction of lactate utilization system in Pseudomonas putida KT2440: a**  
1024                   **novel biocatalyst for l-2-hydroxy-carboxylate production. Sci Rep 4:6939.**

1025   **66.** **Jiang T, Guo X, Yan J, Zhang Y, Wang Y, Zhang M, Sheng B, Ma C, Xu P, Gao C.**

1026       **2017. A Bacterial Multidomain NAD-Independent d-Lactate Dehydrogenase Utilizes**  
1027       **Flavin Adenine Dinucleotide and Fe-S Clusters as Cofactors and Quinone as an**  
1028       **Electron Acceptor for d-Lactate Oxidization.** *J Bacteriol* **199**.

1029       **67. Feller C, Günther R, Hofmann H-J, Grunow M. 2006. Molecular basis of substrate**  
1030       **recognition in D-3-hydroxybutyrate dehydrogenase from *Pseudomonas putida*.**  
1031       **Chembiochem** **7**:1410–1418.

1032       **68. Atsumi S, Hanai T, Liao JC. 2008. Non-fermentative pathways for synthesis of**  
1033       **branched-chain higher alcohols as biofuels.** *Nature* **451**:86–89.

1034       **69. Conrad RS, Massey LK, Sokatch JR. 1974. D- and L-isoleucine metabolism and**  
1035       **regulation of their pathways in *Pseudomonas putida*.** *J Bacteriol* **118**:103–111.

1036       **70. Roberts CM, Conrad RS, Sokatch JR. 1978. The role of enoyl-coa hydratase in the**  
1037       **metabolism of isoleucine by *Pseudomonas putida*.** *Arch Microbiol* **117**:99–108.

1038       **71. Kang A, George KW, Wang G, Baidoo E, Keasling JD, Lee TS. 2016. Isopentenyl**  
1039       **diphosphate (IPP)-bypass mevalonate pathways for isopentenol production.** *Metab*  
1040       **Eng** **34**:25–35.

1041       **72. Sasaki Y, Eng T, Herbert RA, Trinh J, Chen Y, Rodriguez A, Gladden J, Simmons**  
1042       **BA, Petzold CJ, Mukhopadhyay A. 2019. Engineering *Corynebacterium glutamicum***  
1043       **to produce the biogasoline isopentenol from plant biomass hydrolysates.** *Biotechnol*  
1044       **Biofuels** **12**:41.

1045       **73. Hammer SK, Zhang Y, Avalos JL. 2020. Mitochondrial Compartmentalization**  
1046       **Confers Specificity to the 2-Ketoacid Recursive Pathway: Increasing Isopentanol**  
1047       **Production in *Saccharomyces cerevisiae*.** *ACS Synth Biol* **9**:546–555.

1048 74. LaBauve AE, Wargo MJ. 2012. Growth and laboratory maintenance of  
1049 **Pseudomonas aeruginosa**. *Curr Protoc Microbiol Chapter 6:Unit 6E.1*.

1050 75. Ham TS, Dmytryk Z, Plahar H, Chen J, Hillson NJ, Keasling JD. 2012. Design,  
1051 implementation and practice of JBEI-ICE: an open source biological part registry  
1052 platform and tools. *Nucleic Acids Res* 40:e141.

1053 76. Chen J, Densmore D, Ham TS, Keasling JD, Hillson NJ. 2012. DeviceEditor visual  
1054 biological CAD canvas. *J Biol Eng* 6:1.

1055 77. Hillson NJ, Rosengarten RD, Keasling JD. 2012. j5 DNA assembly design automation  
1056 software. *ACS Synth Biol* 1:14–21.

1057 78. Gibson DG, Young L, Chuang R-Y, Venter JC, Hutchison CA, Smith HO. 2009.  
1058 Enzymatic assembly of DNA molecules up to several hundred kilobases. *Nat  
1059 Methods* 6:343–345.

1060 79. Engler C, Kandzia R, Marillonnet S. 2008. A one pot, one step, precision cloning  
1061 method with high throughput capability. *PLoS ONE* 3:e3647.

1062 80. Shanks RMQ, Kadouri DE, MacEachran DP, O'Toole GA. 2009. New yeast  
1063 recombineering tools for bacteria. *Plasmid* 62:88–97.

1064 81. Thompson MG, Pearson AN, Barajas JF, Cruz-Morales P, Sedaghatian N, Costello  
1065 Z, Garber ME, Incha MR, Valencia LE, Baidoo EEK, Martin HG, Mukhopadhyay  
1066 A, Keasling JD. 2020. Identification, Characterization, and Application of a Highly  
1067 Sensitive Lactam Biosensor from *Pseudomonas putida*. *ACS Synth Biol* 9:53–62.

1068 82. George KW, Thompson MG, Kang A, Baidoo E, Wang G, Chan LJC, Adams PD,  
1069 Petzold CJ, Keasling JD, Lee TS. 2015. Metabolic engineering for the high-yield

1070        **production of isoprenoid-based C<sub>5</sub> alcohols in *E. coli*. *Sci Rep* 5:11128.**

1071        **83. Jones E, Oliphant T, Peterson P, Others. SciPy: Open source scientific tools for**  
1072        **Python.**

1073        **84. van der Walt S, Colbert SC, Varoquaux G. 2011. The NumPy Array: A Structure for**  
1074        **Efficient Numerical Computation. *Comput Sci Eng* 13:22–30.**

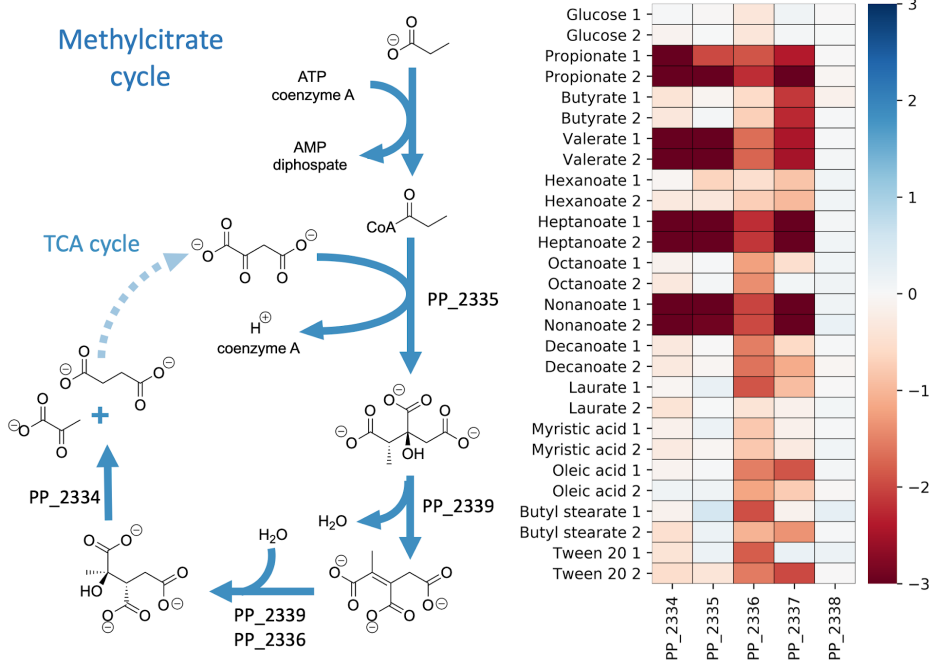
1075        **85. Kalyaanamoorthy S, Minh BQ, Wong TKF, von Haeseler A, Jermiin LS. 2017.**  
1076        **ModelFinder: fast model selection for accurate phylogenetic estimates. *Nat Methods***  
1077        **14:587–589.**

1078        **86. Cruz-Morales P, Ramos-Aboites HE, Licona-Cassani C, Selem-Mójica N, Mejía-**  
1079        **Ponce PM, Souza-Saldívar V, Barona-Gómez F. 2017. Actinobacteria**  
1080        **phylogenomics, selective isolation from an iron oligotrophic environment and**  
1081        **siderophore functional characterization, unveil new desferrioxamine traits. *FEMS***  
1082        ***Microbiol Ecol* 93.**

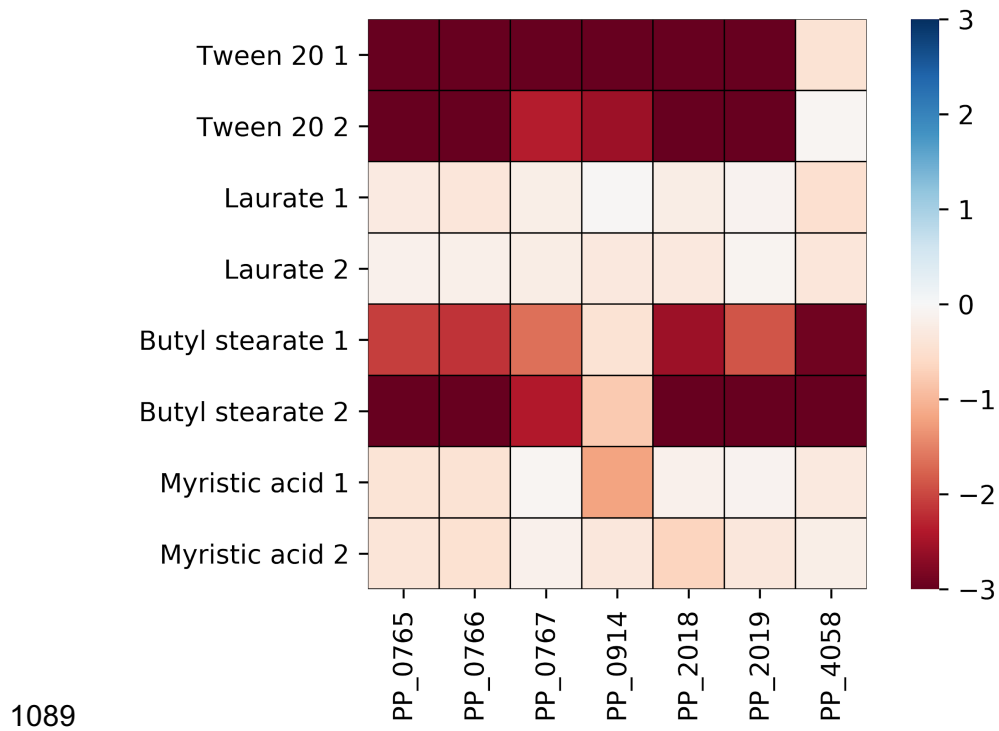
1083

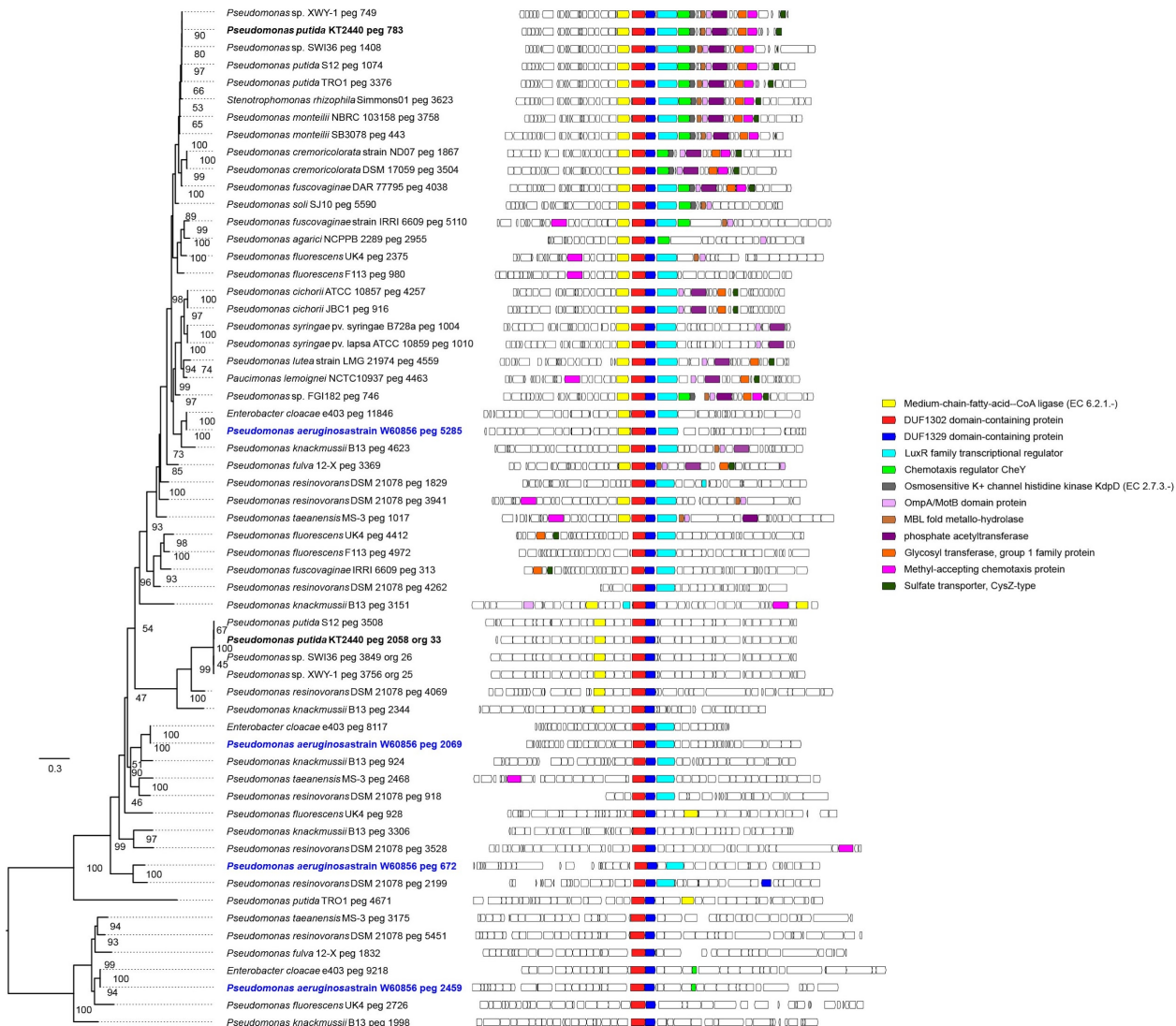
1084        **Supplemental Figures**

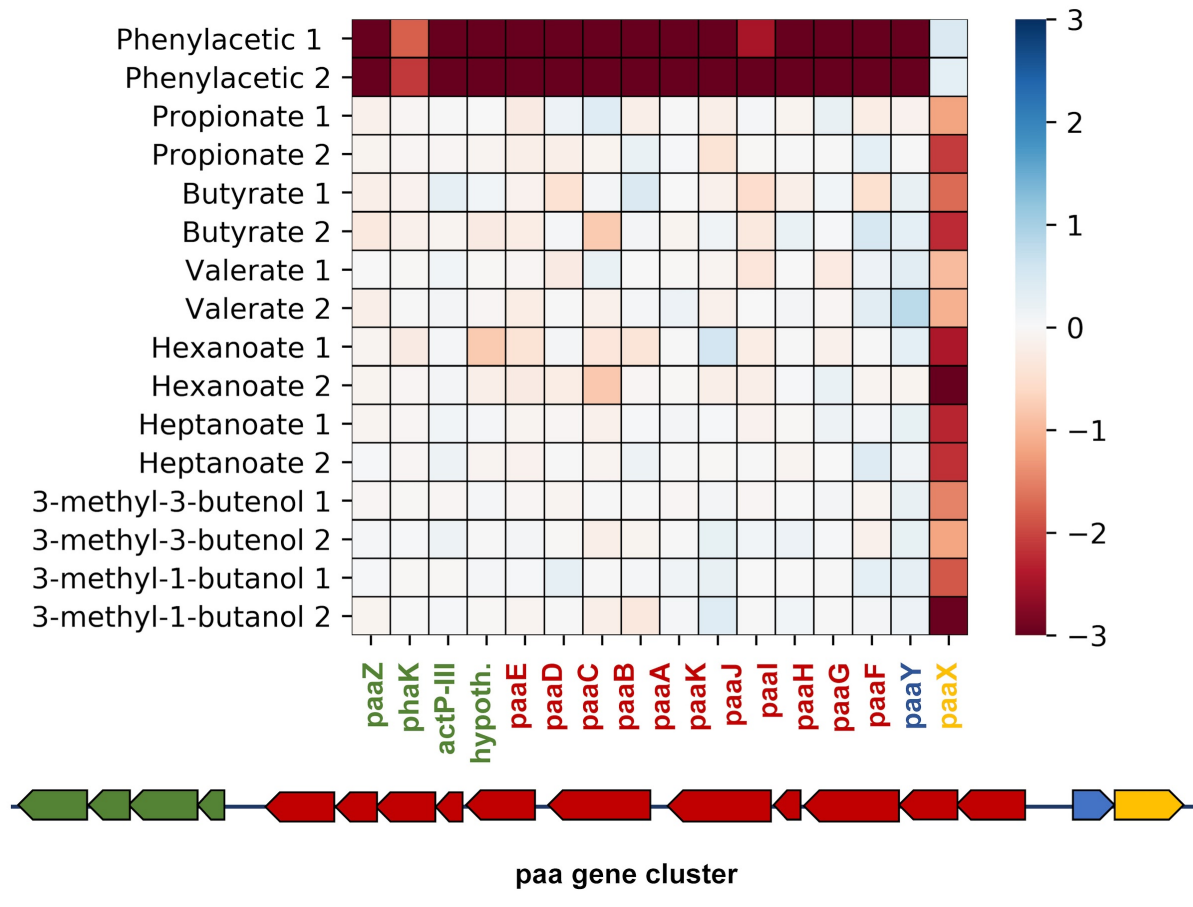
1085



1086 **Figure S1: Fitness scores for genes catalyzing the methylcitrate cycle of *P. putida* KT2440.** Metabolic pathway  
1087 for the MCC of *P. putida* KT2440. Heatmap to the right shows fitness scores for MCC genes when grown on fatty  
1088 acids or glucose. PP\_2337 is predicted to function as an aconitate isomerase not shown in the depiction (left).

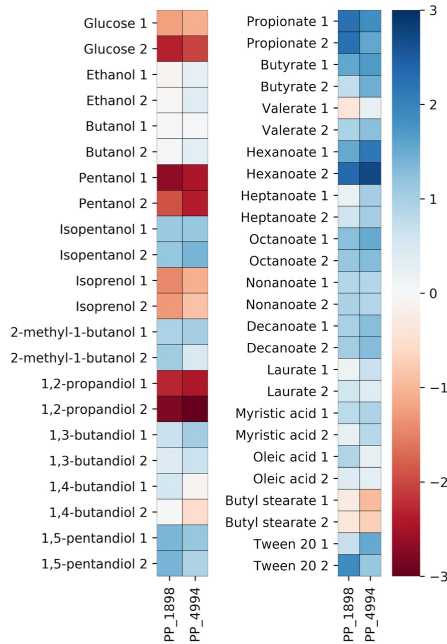






1099

1100 **Figure S4: Detrimental fitness effects on short chain fatty acid catabolism by disrupting *paaX*.** Heatmap shows  
1101 fitness values for the *paa* gene cluster when grown on short chain fatty acids, isoprenol, isopentanol, and  
1102 phenylacetic acid.

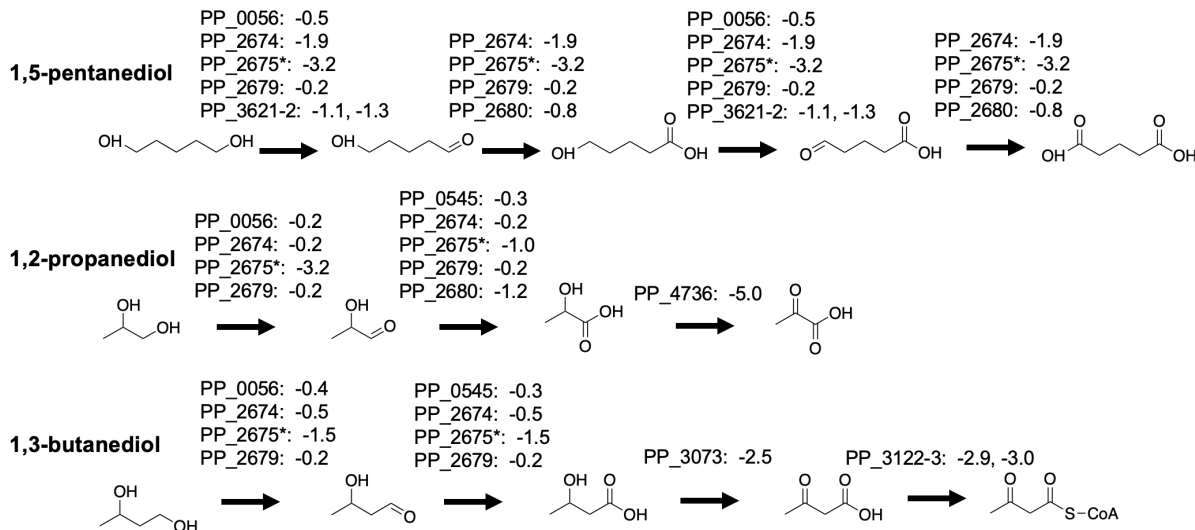


1103

1104 **Figure S5: Fitness profiles of tonB siderophore transporter when grown on fatty acids or alcohols.** Heatmap

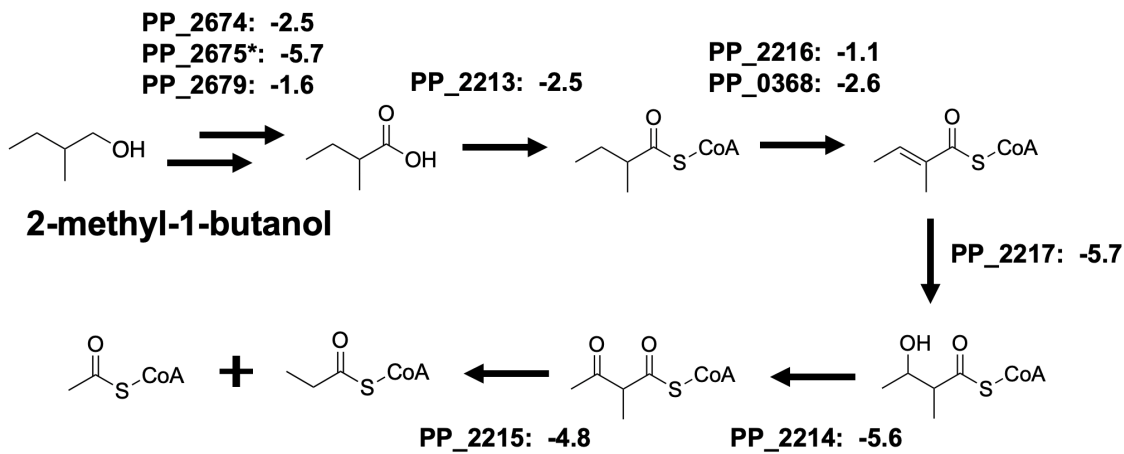
1105 shows fitness scores for PP\_1898, and PP\_4994 on all conditions tested in this work.

1106



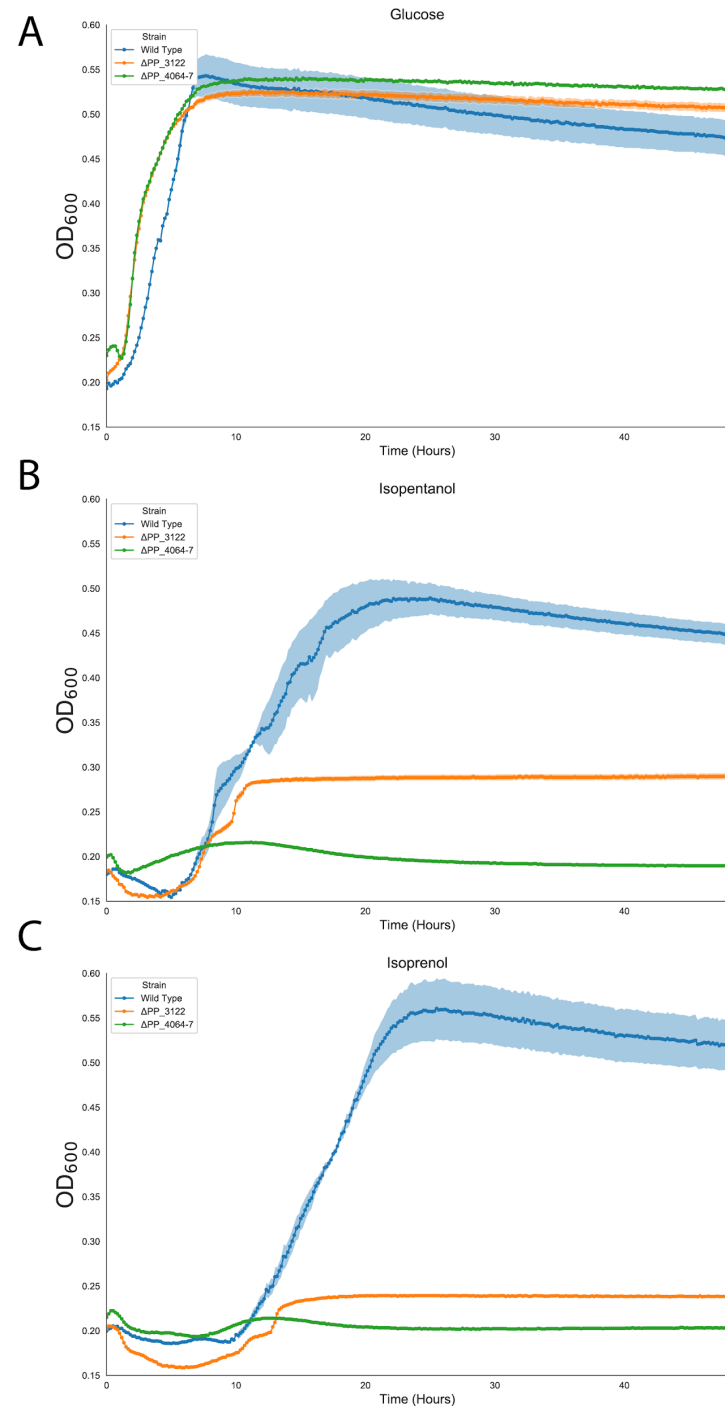
1107

1108 **Figure S6: Putative catabolic pathways for 1,5-pentanediol, 1,2-propanediol, and 1,3-butanediol.** Fitness  
1109 scores for two biological replicates of genes proposed to code for responsible enzymes can be found next to genes.



1110

1111 **Figure S7: Putative catabolic pathway for 2-methyl-1-butanol.** Fitness scores for two biological replicates of  
1112 genes proposed to code for responsible enzymes can be found next to genes.



1113

1114 **Figure S8: Growth of leucine catabolism deletion mutants on branched chain alcohols.** Growth curves of wild-  
1115 type (blue), ΔPP\_3122 (orange), and ΔPP\_4064-4067 (green) strains of *P. putida* on glucose (A), isopentanol (B),  
1116 and isoprenol (C). Shaded area represents 95% CI, n=4.